Supporting Information for

Enhancing Luminescence Properties of Lanthanide(III)/Pyrimidine-4,6-dicarboxylato System by Solvent-free Approach

Javier Cepeda,[a] Sonia Pérez-Yáñez,[a] Garikoitz Beobide,[a] Oscar Castillo,*[a] José Ángel García[b], Mónica Lanchas,[a] and Antonio Luque[a]*

[a] Departamento de Química Inorgánica and [b] Departamento de Física Aplicada II, Facultad de Ciencia y Tecnología, Universidad del País Vasco, Apartado 644, E–48080 Bilbao, Spain

Employed reactants and individual yields

Table S1. Employed reactants.

Name	Formula	CS	AS	MW (g/mol)	CAS	R	S
Cerium(III) nitrate hexahydrate	$Ce(NO_3)_3{\cdot}6H_2O$	Aldrich	≥99%	434.22	10294-41-4	8-41	17-26-39
Dysprosium(III) nitrate hydrate	$Dy(NO_3)_3{\cdot}xH_2O$	Aldrich	≥99%	348.51	100641-13-2	8-36/37/38	17-26-36/37/39
Europium(III) nitrate pentahydrate	$Eu(NO_3)_3{\cdot}5H_2O$	Aldrich	≥99%	428.06	63026-01-7	8-36/37/38	17-26-36/37/39
Erbium(III) nitrate pentahydrate	$Er(NO_3)_3{\cdot}5H_2O$	Aldrich	≥99%	443.35	10031-51-3	8-37/38-41	17-26-36/39
Gadolinium(III) nitrate hexahydrate	$Gd(NO_3)_3{\cdot}6H_2O$	Aldrich	≥99%	451.36	19598-90-4	8-36/37/38	17-26-36/37/39
Holmium(III) nitrate pentahydrate	$Ho(NO_3)_3{\cdot}5H_2O$	Aldrich	≥99%	441.02	14483-18-2	8-36/37/38	17-26-36/37/39
Lanthanum(III) nitrate hexahydrate	$La(NO_3)_3{\cdot}6H_2O$	Aldrich	≥99%	433.01	10277-43-7	8-36/37/38	17-26-36
Lutetium(III) nitrate hydrate	$Lu(NO_3)_3{\cdot}xH_2O$	Aldrich	99.9%	360.98	100641-16-5	8-36/37/38	17-26-36
Neodymium(III) nitrate hexahydrate	$Nd(NO_3)_3{\cdot}6H_2O$	Aldrich	99.9%	438.35	16454-60-7	8-36/37/38	17-26-36/37/39
Praseodymium(III) nitrate hexahydrate	$Pr(NO_3)_3{\cdot}6H_2O$	Aldrich	99.9%	435.01	15878-77-0	8-36/37/38	17-26-36/37/39
Samarium(III) nitrate hexahydrate	$Sm(NO_3)_3{\cdot}6H_2O$	Aldrich	99.9%	444.47	13759-83-6	8-36/37/38	17-26-36/37/39
Terbium(III) nitrate hexahydrate	$Tb(NO_3)_3{\cdot}6H_2O$	Aldrich	99.9%	453.03	13451-19-9	8-36/37/38	17-26-36/37/39
Thulium(III) nitrate hexahydrate	$Tm(NO_3)_3{\cdot}5H_2O$	Aldrich	99.9%	445.03	36548-87-5	8-36/37/38	17-26-36/37/39
Ytterbium(III) nitrate hexahydrate	$Yb(NO_3)_3{\cdot}5H_2O$	Aldrich	99.9%	449.13	35725-34-9	8-36/37/38	17-26-36

Table S2. Yields for all the **1-Ln** compounds.

Compound	**1-La**	**1-Ce**	**1-Pr**	**1-Nd**	**1-Sm**	**1-Eu**
Yield (%)	91.4	94.8	92.3	91.6	90.9	93.3

Table S3. Yields for all the **2-Ln** compounds.

Compound	**2-Gd**	**2-Tb**	**2-Dy**	**2-Ho**	**2-Er**	**2-Tm**	**2-Yb**	**2-Lu**
Yield (%)	94.4	93.9	94.1	91.6	91.3	93.8	94.5	92.8

Table S4. Elemental analyses of **1-Ln** and **2-Ln** compounds.

Compound	C (%)		H (%)		N (%)		Ln (%)	
	Exp.	*Cal.*	*Exp.*	*Cal.*	*Exp.*	*Cal.*	*Exp.*	*Cal.*
$C_6H_4LnN_3O_8$								
1-La	18.92	18.72	1.16	1.05	10.78	10.91	35.95	36.08
1-Ce	18.52	18.66	1.28	1.04	10.73	10.88	36.14	36.28
1-Pr	18.55	18.62	1.19	1.04	10.90	10.86	36.28	36.41
1-Nd	18.29	18.46	1.32	1.03	10.62	10.76	37.11	36.95
1-Sm	18.34	18.18	0.88	1.02	10.76	10.60	37.86	37.93
1-Eu	17.93	18.10	1.22	1.01	10.73	10.56	38.31	38.17
$C_6H_6LnN_3O_9$								
2-Gd	16.88	17.10	1.55	1.44	9.87	9.97	37.43	37.32
2-Tb	16.93	17.03	1.54	1.43	9.98	9.93	37.71	37.57
2-Dy	17.02	16.89	1.56	1.42	9.69	9.85	38.17	38.09
2-Ho	16.67	16.80	1.34	1.41	9.89	9.79	38.46	38.44
2-Er	16.93	16.71	1.45	1.40	9.65	9.74	38.86	38.77
2-Tm	16.51	16.64	1.28	1.40	9.87	9.70	38.89	39.01
2-Yb	16.69	16.48	1.52	1.38	9.55	9.61	39.37	39.58
2-Lu	16.25	16.41	1.20	1.38	9.73	9.57	39.90	39.85

FTIR analysis

All spectra exhibit a broad and intense band around 3530 cm^{-1} that corresponds to the vibration of the O–H bond of free water, followed by weak bands between 3215 and 3085 cm^{-1} corresponding to the C–H vibrations of the pyrimidinic ring of the pmdc. The intense vibrations in the 1670–1520 cm^{-1} region are attributed to both the asymmetric stretching vibrations of the carboxylate groups and the aromatic C–C and C–N bonds, while the symmetric stretching vibrations of the carboxylate groups appear in the lower range of 1405–1285 cm^{-1}. The main difference between spectra of **1-Ln** and **2-Ln** is that most of the bands involving vibrations of carboxylate groups and the pyrimidine ring are shifted towards lower wavenumbers for the **1-Ln** family, which could be attributed to the different coordination mode of pmdc. Vibrations corresponding to the nitrato anions are also distinguished within the last frequency region. In good agreement to the results obtained by Gatehouse el al.,[1] the bidentate coordination mode of the nitrate anion is ensured by the presence of three bands at 1476, 1290, and 1025 cm^{-1} with a separation between the two highest-frequency bands of 186 cm^{-1}. These latter bands are present in all spectra although they partially overlap those of pmdc ligand. Moreover, there is no evidence of free nitrate anions in the sample (coming from unreacted lanthanide(III) nitrates) due to the lack of the 1383 cm^{-1} band. At lower frequencies, the remaining bands are attributed to the distortions originated in the aromatic ring and the carboxylate groups of the pmdc ligand. The vibration bands of the M–O and M–N bonds are observed below 530 cm^{-1}.

(1) (a) Gatehouse, B. M.; Livinstone, S. E.; Nyholm, R. S. *J. Chem. Soc.* **1957**, 4222. (b) Gatehouse, B. M.; Livinstone, S. E.; Nyholm, R. S. *J. Inorg. Nucl. Chem.* **1958**, *8*, 75. (c) Nakamoto, K. *Infrared spectra of inorganic and coordination compounds*; John Wiley & Sons, **1997**.

Table S5. Observed bands (cm^{-1}) for selected compounds of the isostructural **1-Ln** and **2-Ln** series.[a]

Assignment[b]	*1-La*	*2-Gd*
ν (O–H)	3530m, 3410m	3530m, 3470m
ν (C–H)	3215m, 3115m, 3085m	3190m, 3135m
ν_{as}(O–C–O) + ν (C=C + C=N)	1640vs, 1625vs, 1615vs, 1610s, 1550s, 1520w	1670vs, 1655vs, 1640vs, 1600s, 1550s, 1520s
ν (C_{ar}–C)	1475m, 1445m	1500s, 1485m, 1445m
ν_{s} (O–C–O)	1390vs, 1325sh, 1315s, 1285w	1405vs, 1315m, 1290s
ν (NO_3)	1475m, 1285w, 1020m	1485w, 1290s, 1030m
δ_{ip}(C–H)	1210w, 1195m, 1110m, 1035m, 1020m	1275s, 1195m, 1095m, 1030m, 1005w, 995w
δ_{op}(C–H)	960m, 950m, 920m	960w, 915w
δ_{ring}	855m	855m
δ_{ip}(O–C–O)	820m, 745s	810m, 740m
δ_{op}(O–C–O)	720m, 700m, 670w	725m, 720m, 705m, 615s
τ_{ring}	590w	585m, 530m
ν (M–O + M–N)	520m, 490w, 470w	460w

[a] vs: very strong, s: strong, m: medium, w: weak, sh: shoulder. [b] ν: stretching, δ: bending, ip: in plane, op: out of plane, s: symmetric, as: asymmetric.

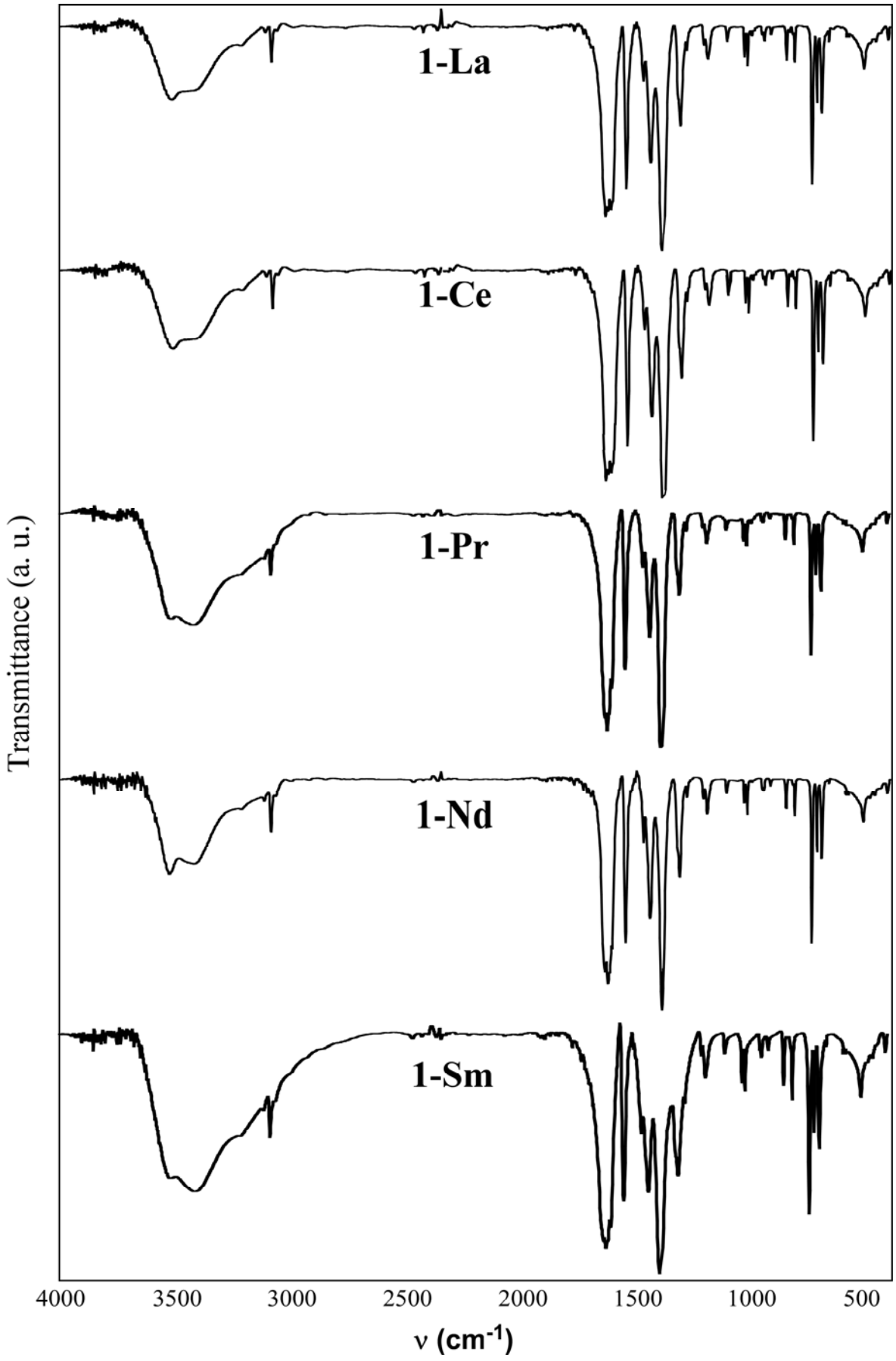

Figure S1. FTIR spectra of some **1-Ln** compounds.

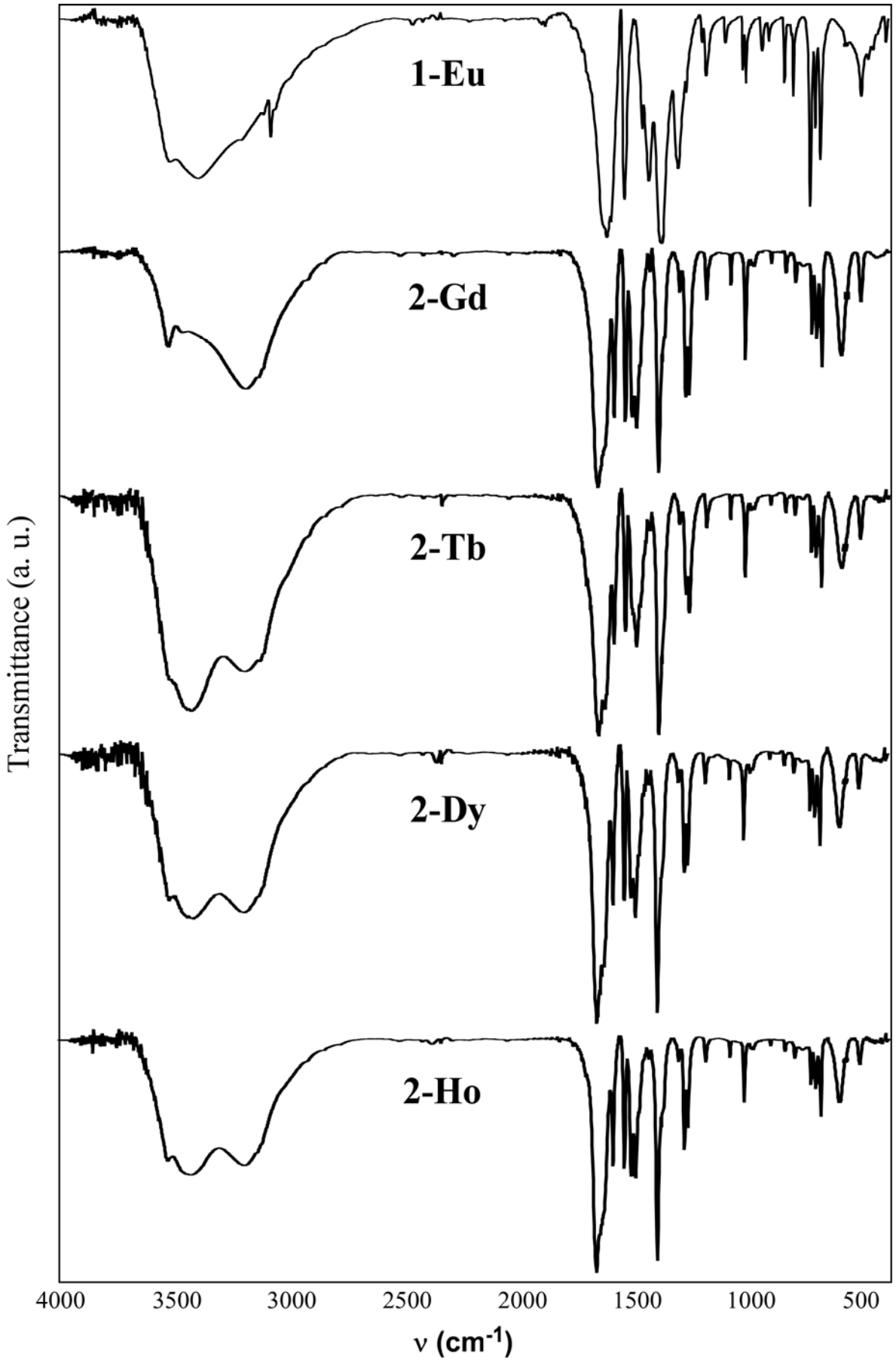

Figure S2. FTIR spectra of some **1-Ln** and **2-Ln** compounds.

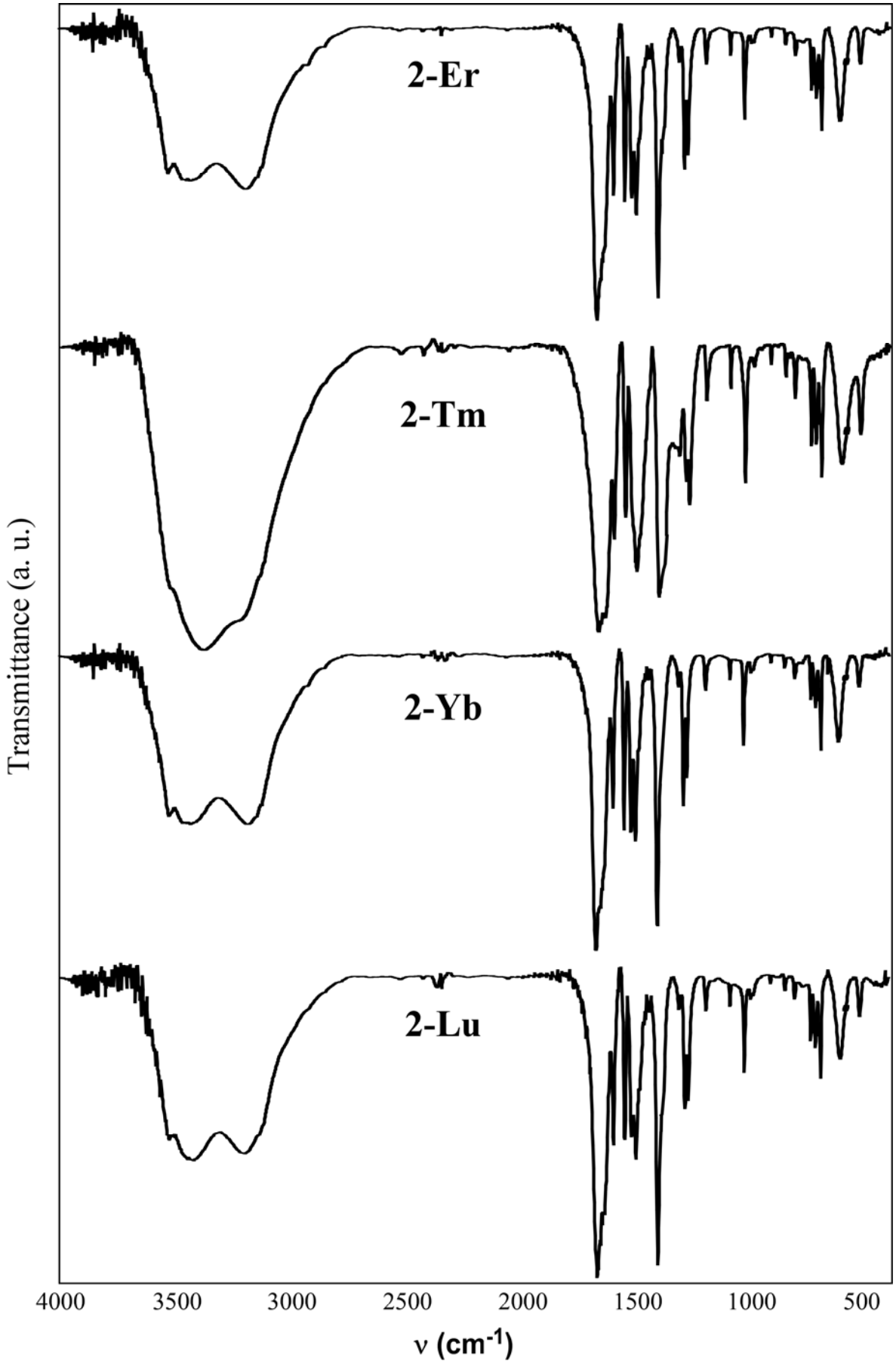

Figure S3. FTIR spectra of the remaining **2-Ln** compounds.

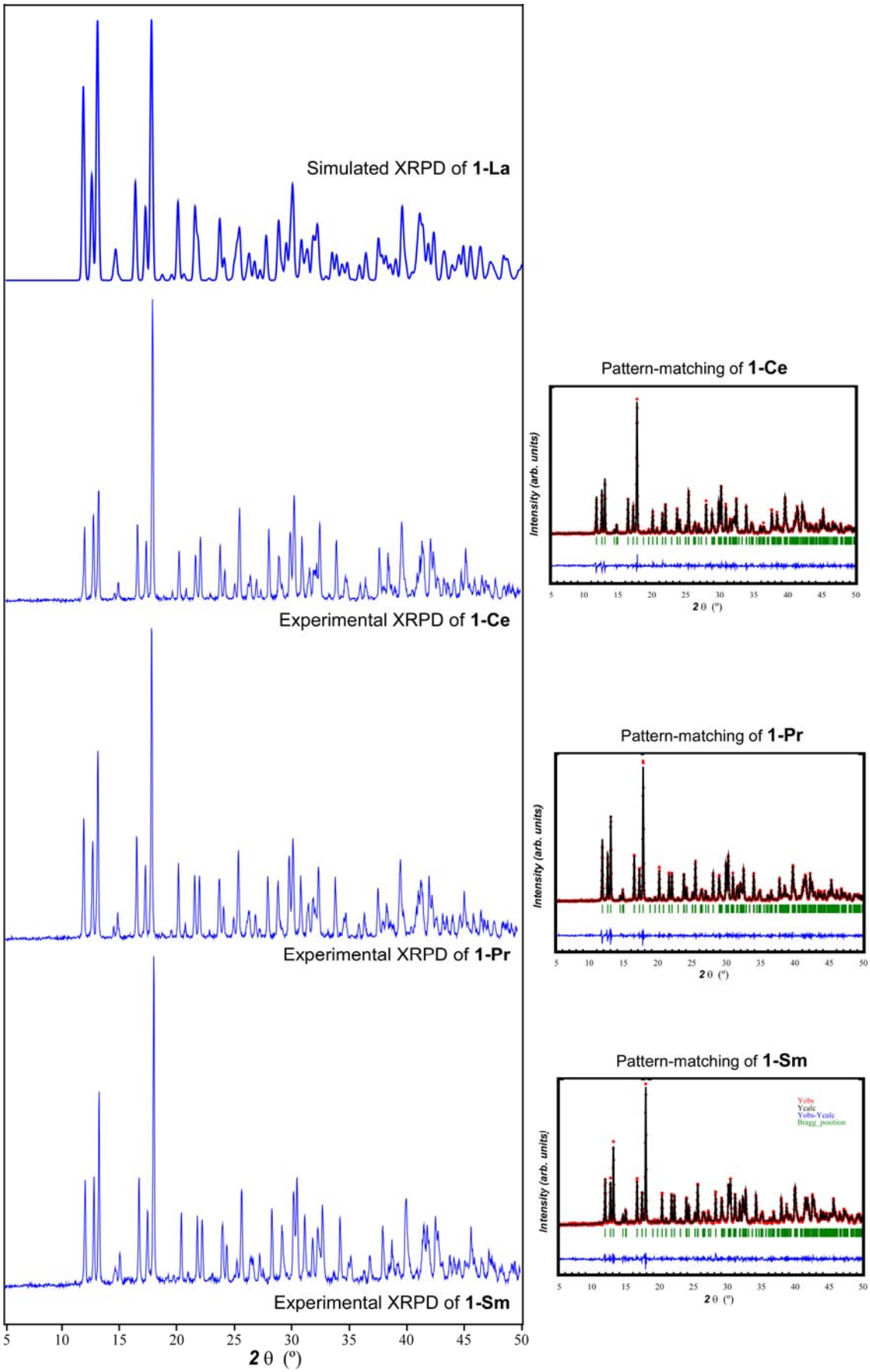

Figure S4. Pattern-matching analyses and experimental XRPD of **1-Ln** compounds.

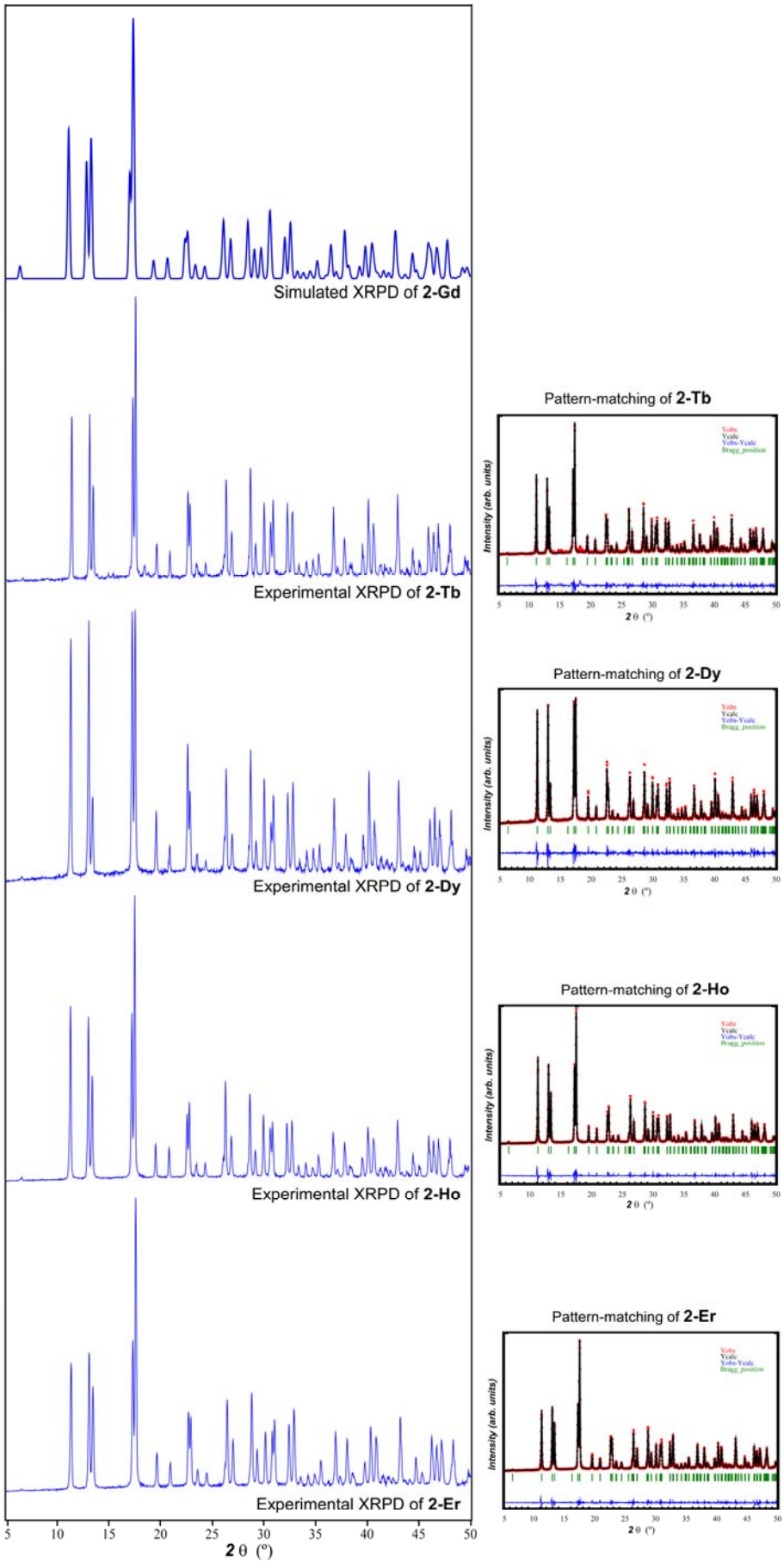

Figure S5. Pattern-matching analyses and experimental XRPD of some **2-Ln** compounds.

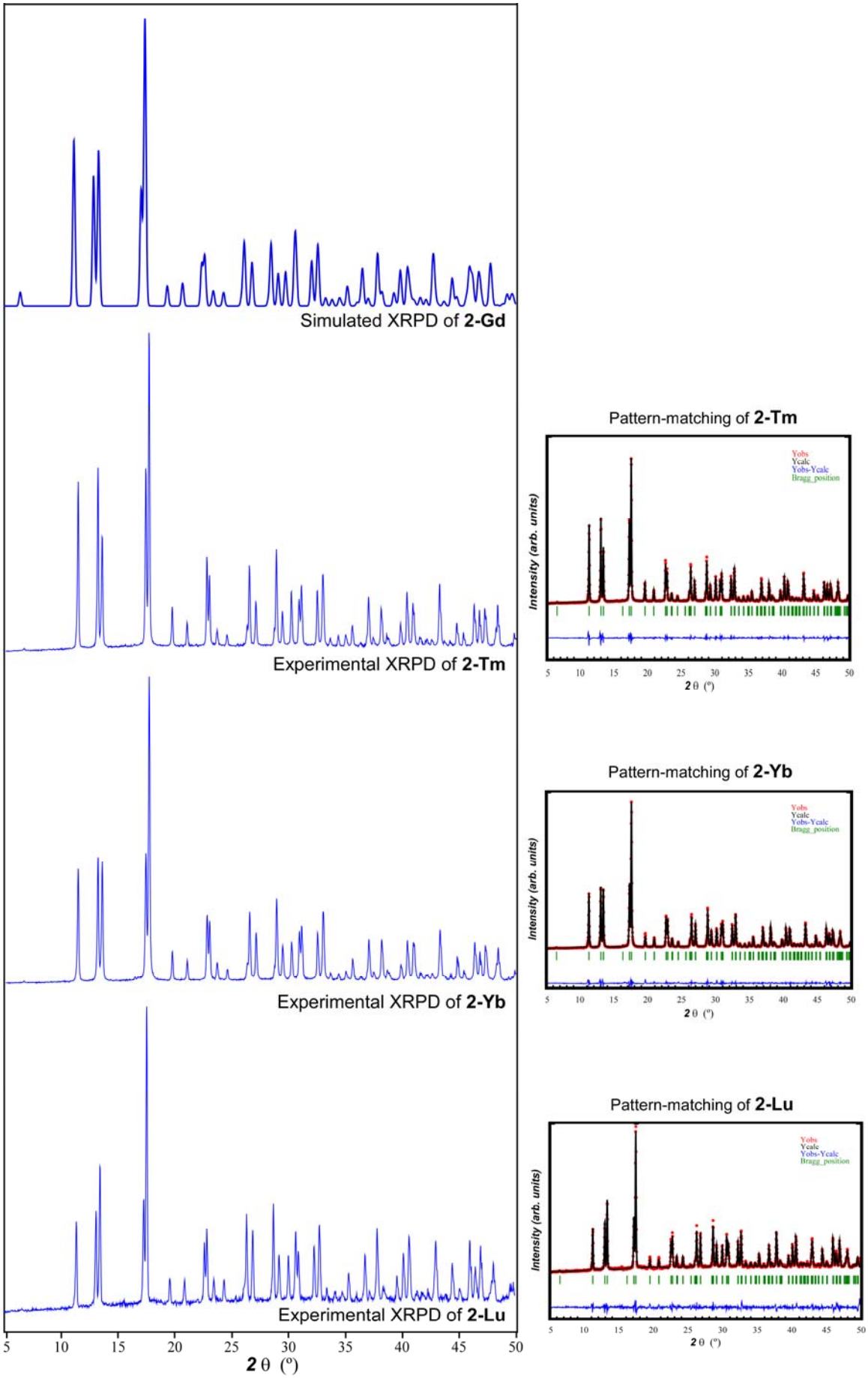

Figure S6. Pattern-matching analyses and experimental XRPD of **2-Ln** compounds (cont.).

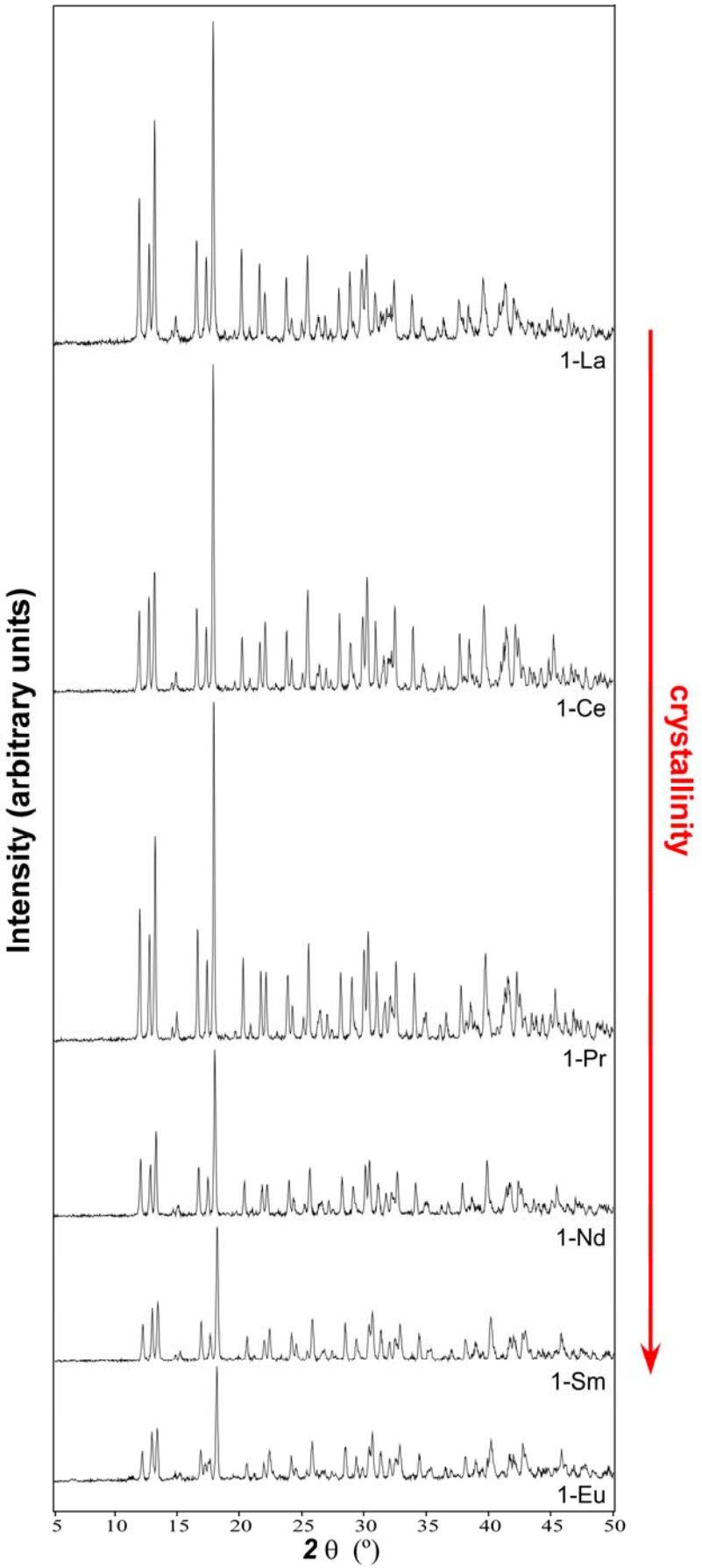

Figure S7. Decrease in the crystallinity observed for XRPD patterns of compounds synthesised at 140 ºC.

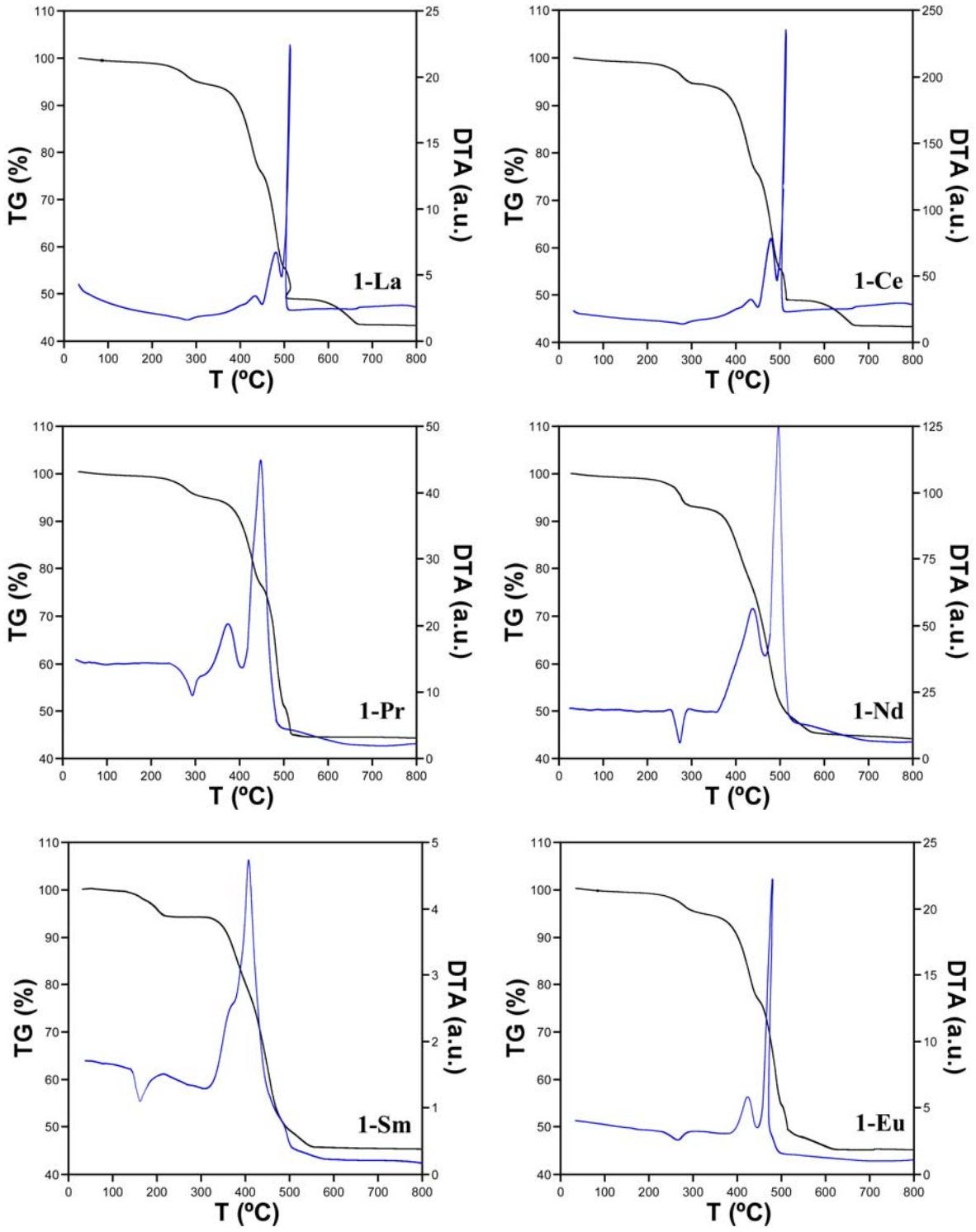

Figure S8. Thermogravimetric measurements of all **1-Ln** compounds.

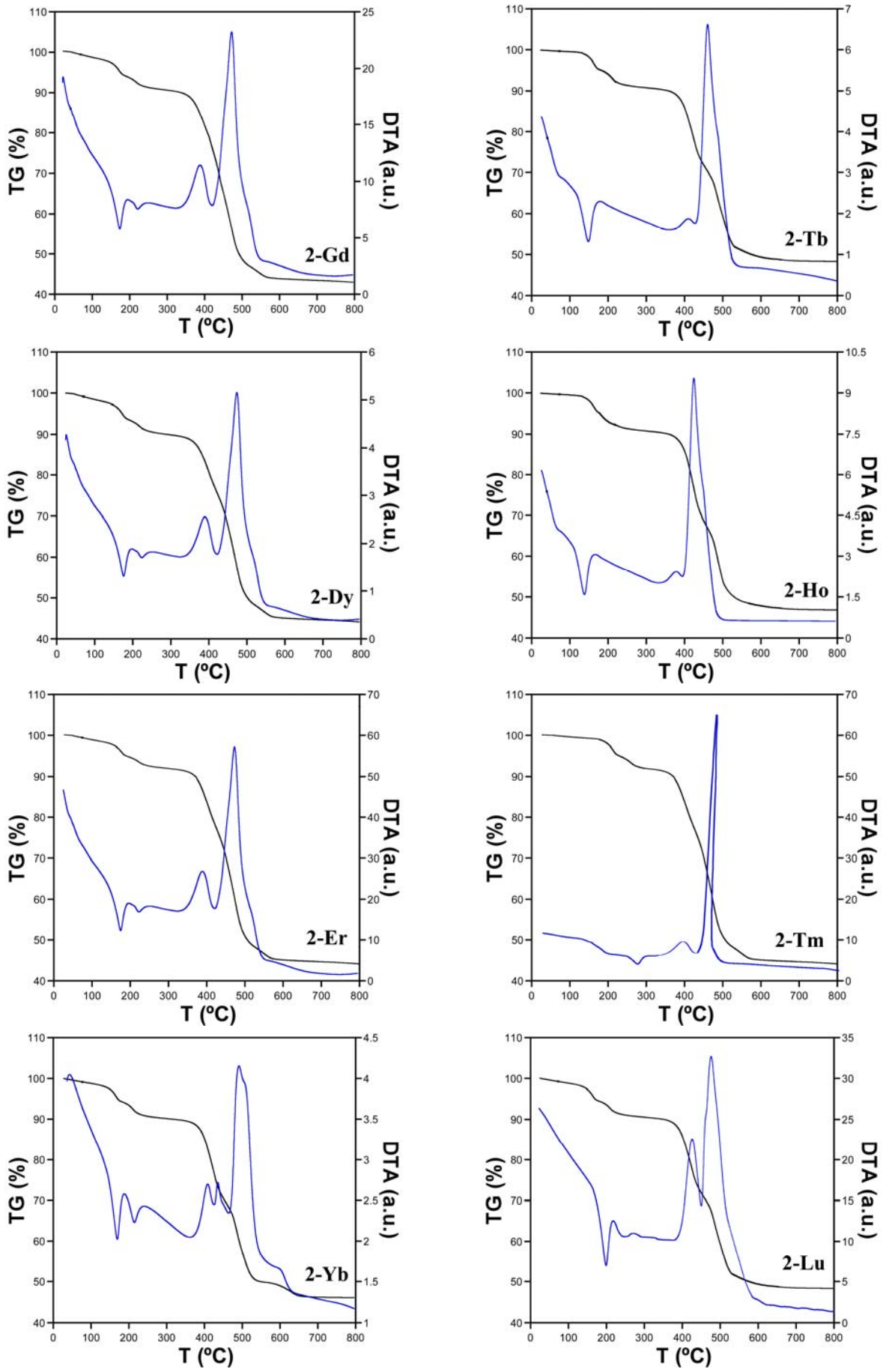

Figure S9. Thermogravimetric measurements of **2-Ln** compounds.

Table S6. Thermal evolution of the visible emission lifetime values of **1-Ln** and **2-Ln** compounds.

Step	*Ti*	*Tf*	*Tpeak*	*Δm(%)*	*ΔH*	*ΣΔm(%)*	*$ΣΔm_{teor}$(%)*
1-Ln							
1	230	325	280	5.0	Endo	5.0	4.7 (–1H_2O)
2	350	450	430	19.0	Exo	24.0	
3	450	495	480	20.0	Exo	44.0	
4	495	515	510	6.1	Exo	50.1	
5	570	680	590	6.4	Exo	56.5	57.7 (La_2O_3)
2-Ln							
1	25	190	175	6.3	Endo	6.3	4.2 (–1H_2O)
2	190	260	220	3.7	Endo	10.0	8.4 (–1H_2O)
3	320	420	390	13.7	Exo	23.7	
4	420	575	475	32.2	Exo	55.9	56.3 (Dy_2O_3)

[a] Ti = initial temperature; Tf = final temperature; Tpeak = DTA peak temperature; Δm(%) = mass loss percentage for each process; ΔH = process type in the basis of DTA; ΣΔm(%) = total mass loss percentage; $ΣΔm(\%)_{teor}$ = theoretical total mass loss percentage. [b] Released water molecules and final residue by compound formula.

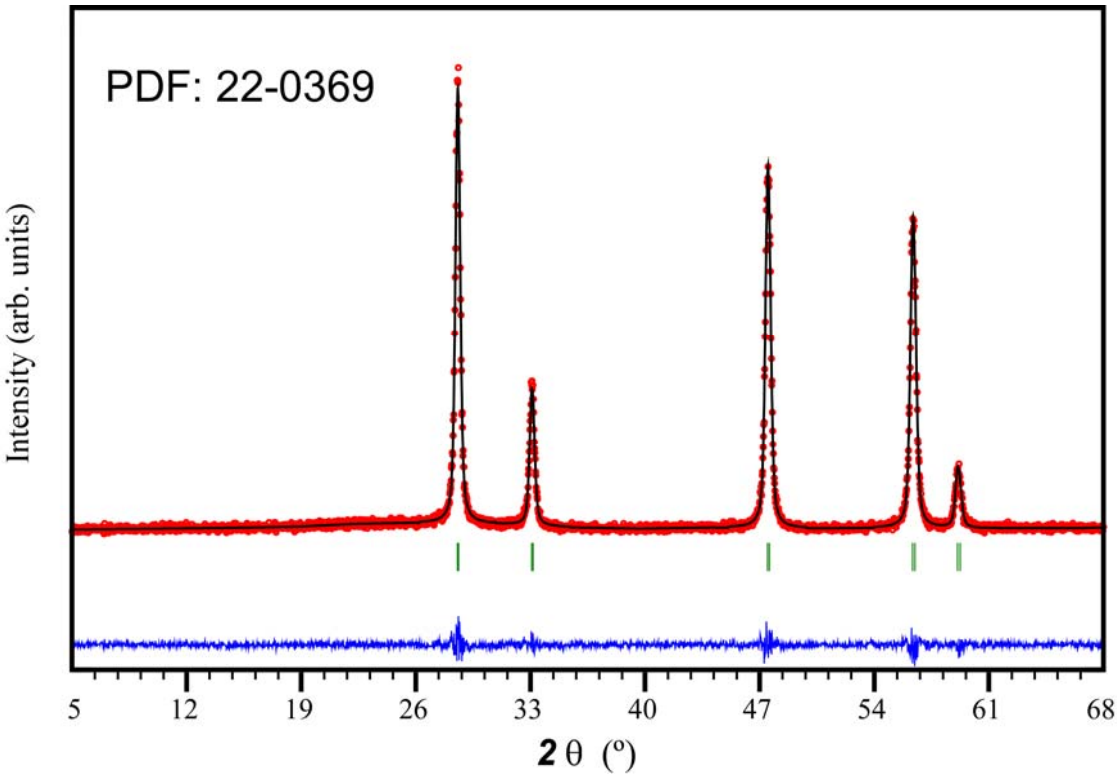

Figure S10. Pattern-matching refinement of the La_2O_3 thermogravimetric residue.

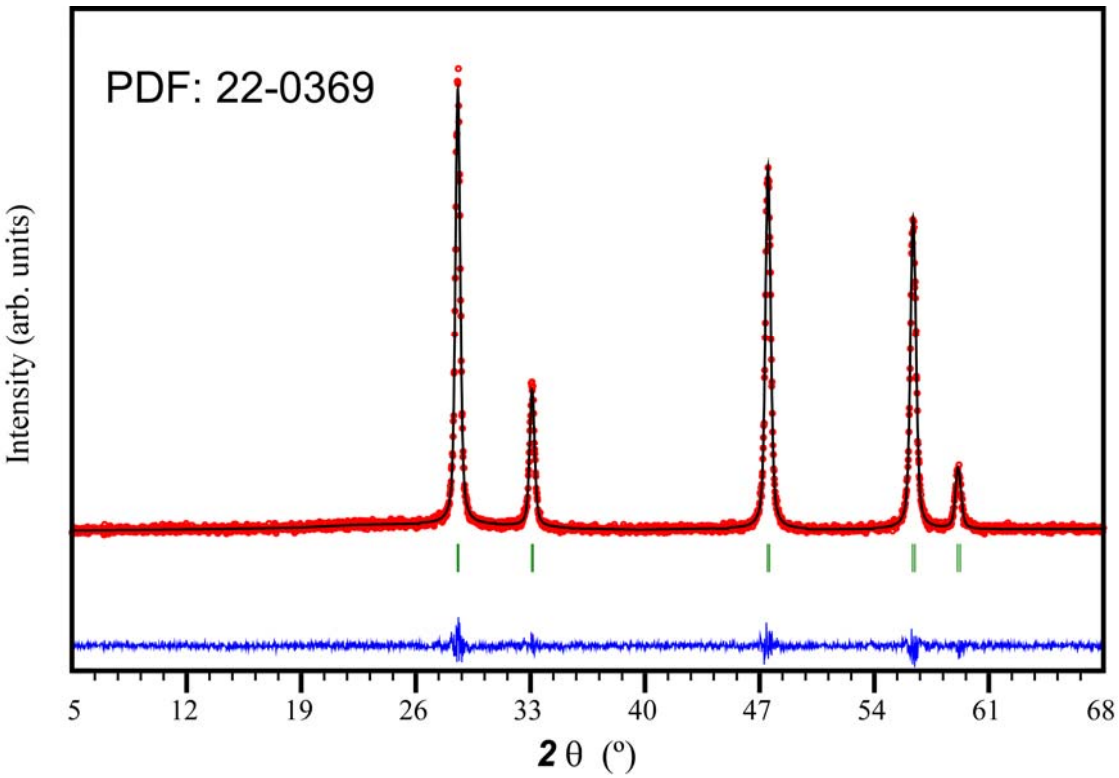

Figure S11. Pattern-matching refinement of the Gd_2O_3 thermogravimetric residue.

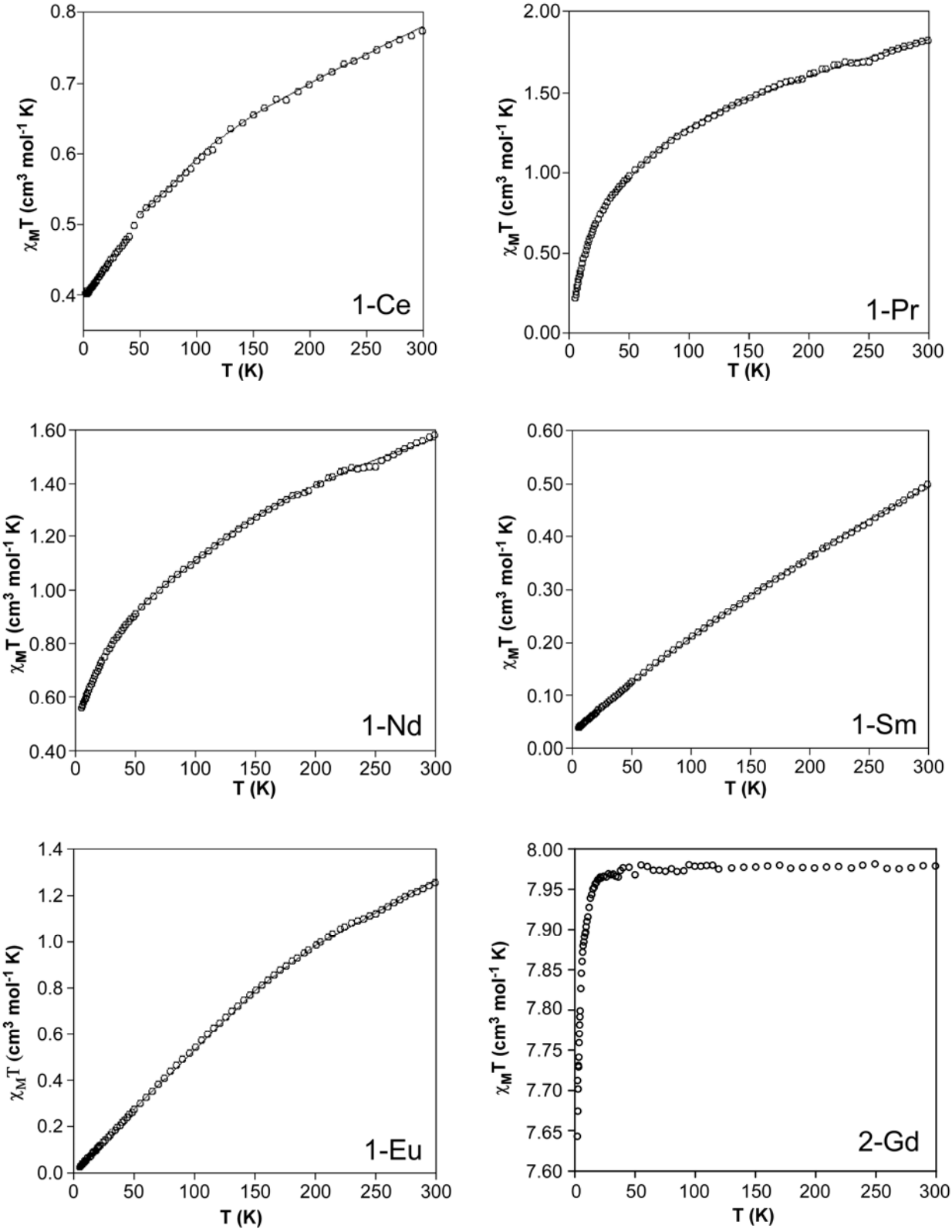

Figure S12. Plots of the thermal dependence of the magnetic susceptibility of **1-Ln** and **2-Ln** compounds. (o) and the best theoretical fit (–).

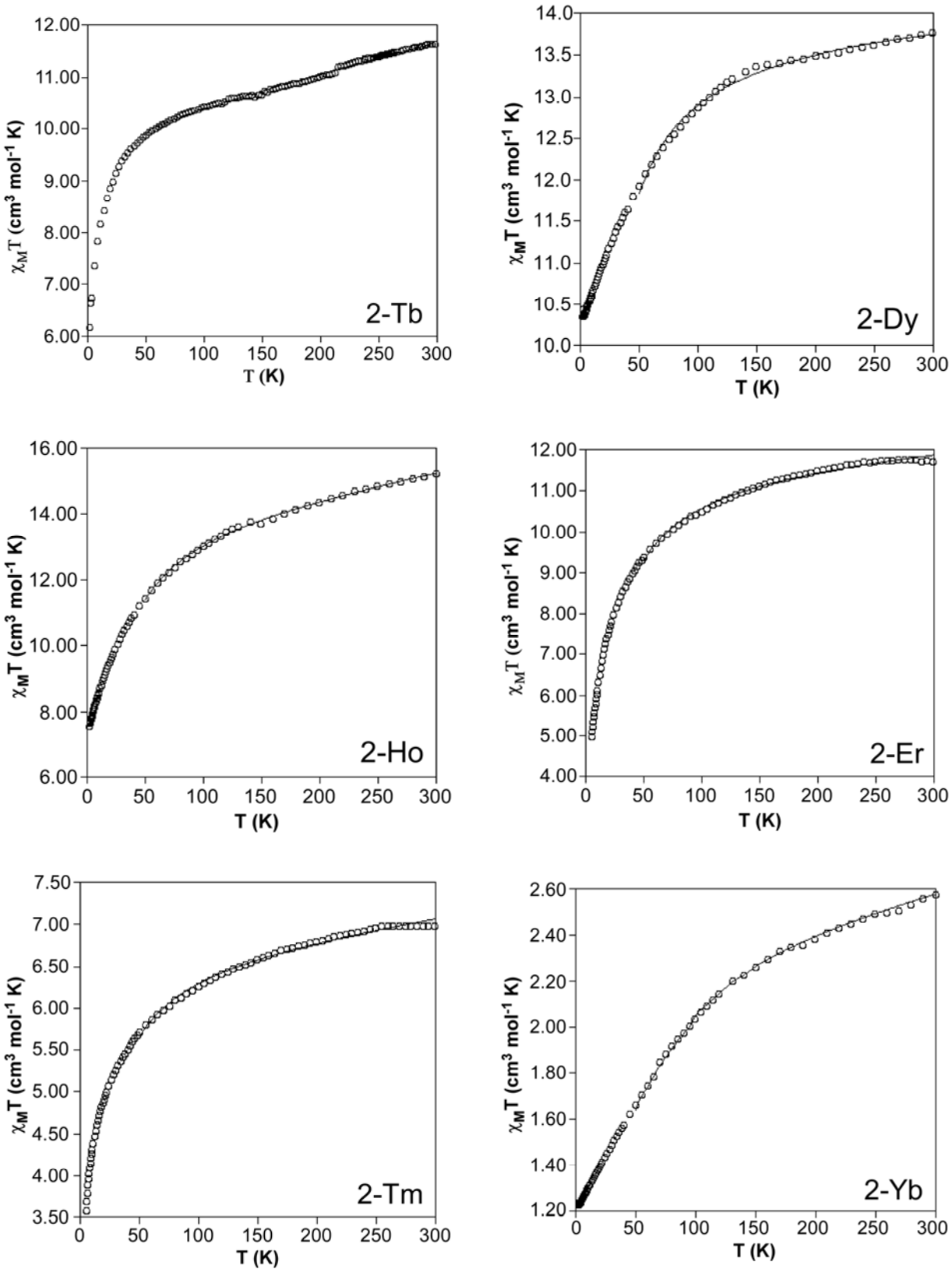

Figure S13. Plots of the thermal dependence of the magnetic susceptibility of **1-Ln** and **2-Ln** compounds. (o) and the best theoretical fit (–) (cont.).

$$\chi_{Ce} = \frac{Ng^2\beta^2}{kT}\frac{50/4e^{-25\Delta/4kT} + 18/4e^{-9\Delta/4kT} + 1/2e^{-\Delta/4kT}}{2e^{-25\Delta/4kT} + 2e^{-9\Delta/4kT} + 2e^{-\Delta/4kT}}$$

$$\chi_{\mathrm{Pr}} = \frac{Ng^2\beta^2}{kT}\frac{2e^{-\Delta/kT} + 8e^{-4\Delta/kT} + 18e^{-9\Delta/kT} + 32e^{-16\Delta/kT}}{1 + 2e^{-\Delta/kT} + 2e^{-4\Delta/kT} + 2e^{-9\Delta/kT} + 2e^{-16\Delta/kT}}$$

$$\chi_{Nd} = \frac{Ng^2\beta^2}{4kT}\frac{81e^{-81\Delta/4kT} + 49e^{-49\Delta/4kT} + 25e^{-25\Delta/4kT} + 9e^{-9\Delta/4kT} + e^{-9\Delta/4kT}}{e^{-81\Delta/4kT} + e^{-49\Delta/4kT} + e^{-25\Delta/4kT} + e^{-9\Delta/4kT} + e^{-9\Delta/4kT}}$$

$$\chi_{Sm} = \frac{N\beta^2}{3kTx}\left(\frac{2.143x + 7.347 + (42.92x + 1.641)e^{-7x/2} + (283.7x - 0.6571)e^{-8x}}{3 + 4e^{-7x/2} + 5e^{-8x} + 6e^{-27x/2} + 7e^{-20x} + 8e^{-55x/2}}\right.$$
$$\left. + \frac{(620.6x - 1.94)e^{-27x/2} + (1122x - 2.835)e^{-20x} + (1813x - 3.556)e^{-55x/2}}{3 + 4e^{-7x/2} + 5e^{-8x} + 6e^{-27x/2} + 7e^{-20x} + 8e^{-55x/2}}\right)$$

$$\chi_{Eu} = \frac{N\beta^2}{3kTx}\left(\frac{24 + (27x - 3)/2e^{-x} + (135x - 5)/2e^{-3x} + (189x - 7/2)e^{-6x}}{1 + 3e^{-x} + 5e^{-3x} + 7e^{-6x} + 9e^{-10x} + 11e^{-15x} + 13e^{-21x}}\right.$$
$$\left. + \frac{(405x - 9/2)e^{-10x} + (1485x - 11)/2e^{-27x} + (2457x - 13)2e^{-21x}}{1 + 3e^{-x} + 5e^{-3x} + 7e^{-6x} + 9e^{-10x} + 11e^{-15x} + 13e^{-21x}}\right)$$

$$\chi_{Gd} = \frac{Ng^2\beta^2}{3kT}\frac{S(S+1)(W_1 + W_2)}{(1-u^2)^2}$$

$$\chi_{Tb} = \frac{Ng^2\beta^2}{kT}\frac{2e^{-\Delta/kT} + 4e^{-2\Delta/kT} + 18e^{-9\Delta/kT} + 32e^{-16\Delta/kT} + 50e^{-25\Delta/kT} + 72e^{-36\Delta/kT}}{1 + 2e^{-\Delta/kT} + 2e^{-2\Delta/kT} + 2e^{-9\Delta/kT} + 2e^{-16\Delta/kT} + 2e^{-25\Delta/kT} + 2e^{-36\Delta/kT}}$$

$$\chi_{Dy} = \frac{Ng^2\beta^2}{kT}\left(\frac{0.5e^{-0.25\Delta/kT} + 4.5e^{-2.25\Delta/kT} + 12.5e^{-6.25\Delta/kT} + 24.5e^{-12.25\Delta/kT}}{1 + 2e^{-\Delta/kT} + 2e^{-2\Delta/kT} + 2e^{-9\Delta/kT} + 2e^{-16\Delta/kT} + 2e^{-25\Delta/kT} + 2e^{-36\Delta/kT}} + \right.$$
$$\left. \frac{40.5e^{-20.25\Delta/kT} + 60.5e^{-30.25\Delta/kT} + 84.5e^{-42.25\Delta/kT} + 112.5e^{-56.25\Delta/kT}}{1 + 2e^{-\Delta/kT} + 2e^{-2\Delta/kT} + 2e^{-9\Delta/kT} + 2e^{-16\Delta/kT} + 2e^{-25\Delta/kT} + 2e^{-36\Delta/kT}}\right)$$

$$\chi_{Ho} = \frac{Ng^2\beta^2}{kT}$$
$$\left(\frac{2e^{-\Delta/kT} + 8e^{-4\Delta/kT} + 18e^{-9\Delta/kT} + 32e^{-16\Delta/kT} + 50e^{-25\Delta/kT} + 72e^{-36\Delta/kT} + 98e^{-49\Delta/kT} + 128e^{-64\Delta/kT}}{1 + 2e^{-\Delta/kT} + 2e^{-4\Delta/kT} + 2e^{-9\Delta/kT} + 2e^{-16\Delta/kT} + 2e^{-25\Delta/kT} + 2e^{-36\Delta/kT} + 2e^{-49\Delta/kT} + 2e^{-64\Delta/kT}}\right)$$

$$\chi_{Er} = \frac{Ng^2\beta^2}{kT}\left(\frac{0.5e^{-0.25\Delta/kT} + 4.5e^{-2.25\Delta/kT} + 12.5e^{-6.25\Delta/kT} + 24.5e^{-12.25\Delta/kT}}{1 + 2e^{-\Delta/kT} + 2e^{-2\Delta/kT} + 2e^{-9\Delta/kT} + 2e^{-16\Delta/kT} + 2e^{-25\Delta/kT} + 2e^{-36\Delta/kT}} + \right.$$
$$\left. \frac{40.5e^{-20.25\Delta/kT} + 60.5e^{-30.25\Delta/kT} + 84.5e^{-42.25\Delta/kT} + 112.5e^{-56.25\Delta/kT}}{1 + 2e^{-\Delta/kT} + 2e^{-2\Delta/kT} + 2e^{-9\Delta/kT} + 2e^{-16\Delta/kT} + 2e^{-25\Delta/kT} + 2e^{-36\Delta/kT}}\right)$$

$$\chi_{Tm} = \frac{Ng^2\beta^2}{kT}\left(\frac{2e^{-\Delta/kT} + 4e^{-2\Delta/kT} + 18e^{-9\Delta/kT} + 32e^{-16\Delta/kT} + 50e^{-25\Delta/kT} + 72e^{-36\Delta/kT}}{1 + 2e^{-\Delta/kT} + 2e^{-2\Delta/kT} + 2e^{-9\Delta/kT} + 2e^{-16\Delta/kT} + 2e^{-25\Delta/kT} + 2e^{-36\Delta/kT}}\right)$$

$$\chi_{Yb} = \frac{Ng^2\beta^2}{kT}\left(\frac{0.5e^{-0.25\Delta/kT} + 1.5e^{-0.75\Delta/kT} + 2.5e^{-1.125\Delta/kT} + 3.5e^{-1.75\Delta/kT}}{2e^{-0.25\Delta/kT} + 2e^{-0.75\Delta/kT} + 2e^{-1.125\Delta/kT} + 2e^{-1.75\Delta/kT}}\right)$$

Scheme S1. Mathematical expressions describing the temperature dependence of the magnetic susceptibility due to the depopulation of the excited Stark levels.

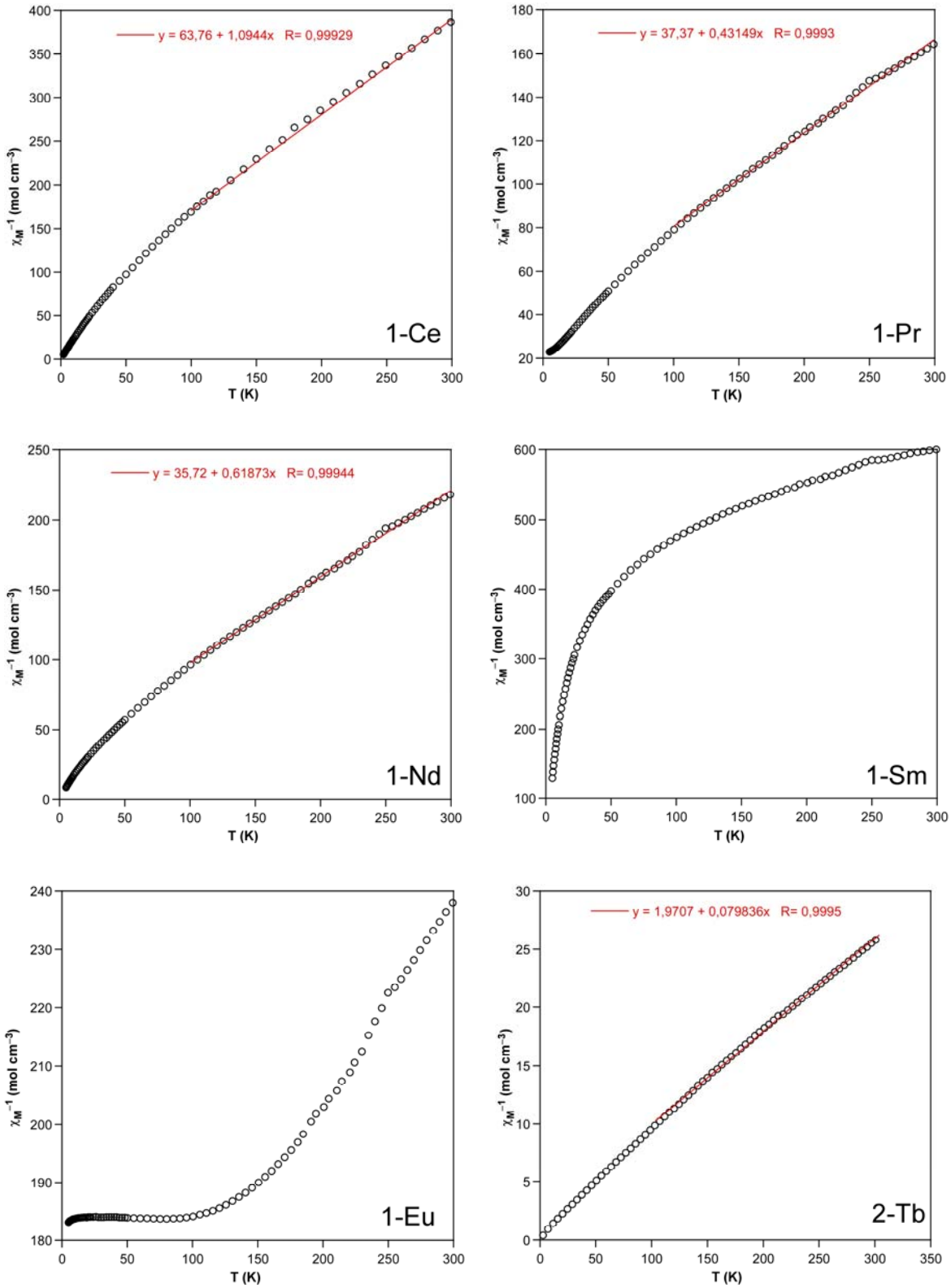

Figure S14. Curie-Weiss fit of the χ_M^{-1} *vs T* curves of **1-Ln** and **2-Ln** compounds.

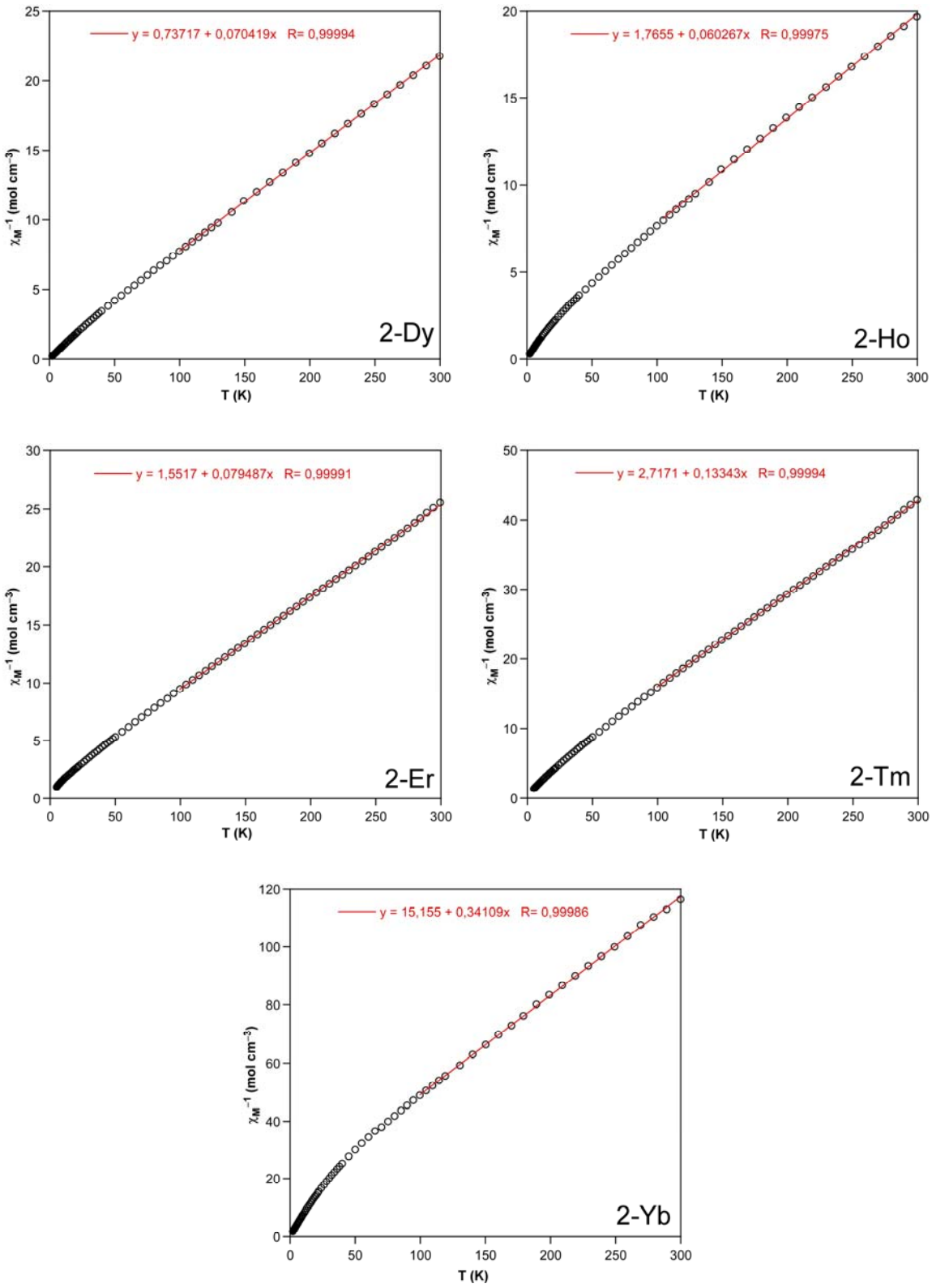

Figure S14. Curie-Weiss fit of the χ_M^{-1} *vs T* curves of **1-Ln** and **2-Ln** compounds (cont.).

Table 7. Best least-squares fits of the experimental magnetic data.[a]

Compound	**g**	**Δ (cm^{-1})**	**C / θ**
1-Ce	0.84	5.15	0.91 / –58.26
1-Pr	0.76	3.02	2.32 / –86.61
1-Nd	0.72	2.51	1.62 / –57.73
2-Tb	1.45	0.10	12.53 / –24.68
2-Dy	1.30	0.34	14.20 / –10.47
2-Ho	1.24	0.40	16.59 / –29.29
2-Er	1.22	0.48	12.58 / –19.52
2-Tm	1.13	0.56	7.49 / –20.36
2-Yb	1.12	3.12	2.93 / –44.43
Compound	g	λ (cm^{-1})	
1-Sm	0.28	235	
1-Eu	5.01	365	

[a] Δ is the zero-field splitting parameter, λ is the spin-orbit coupling parameter, C is the Curie constant and θ corresponds to the Weiss parameter for intermolecular interactions. **1-Sm** and **1-Eu** compounds do not follow the Curie-Weiss law due to the thermal population of the excited states.

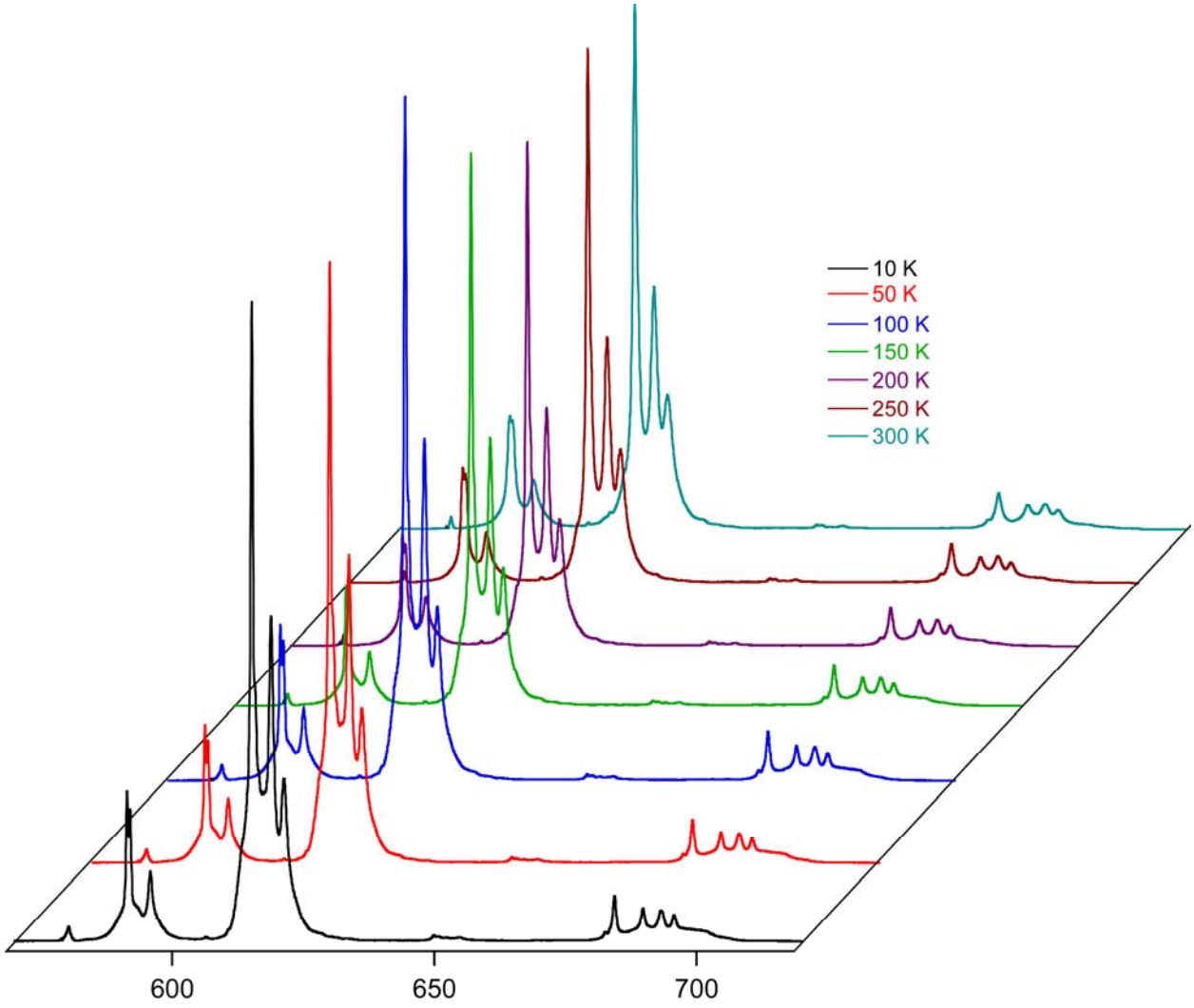

Figure S15. Thermal evolution of the emission spectrum of **1-Eu** excited at 325 nm.

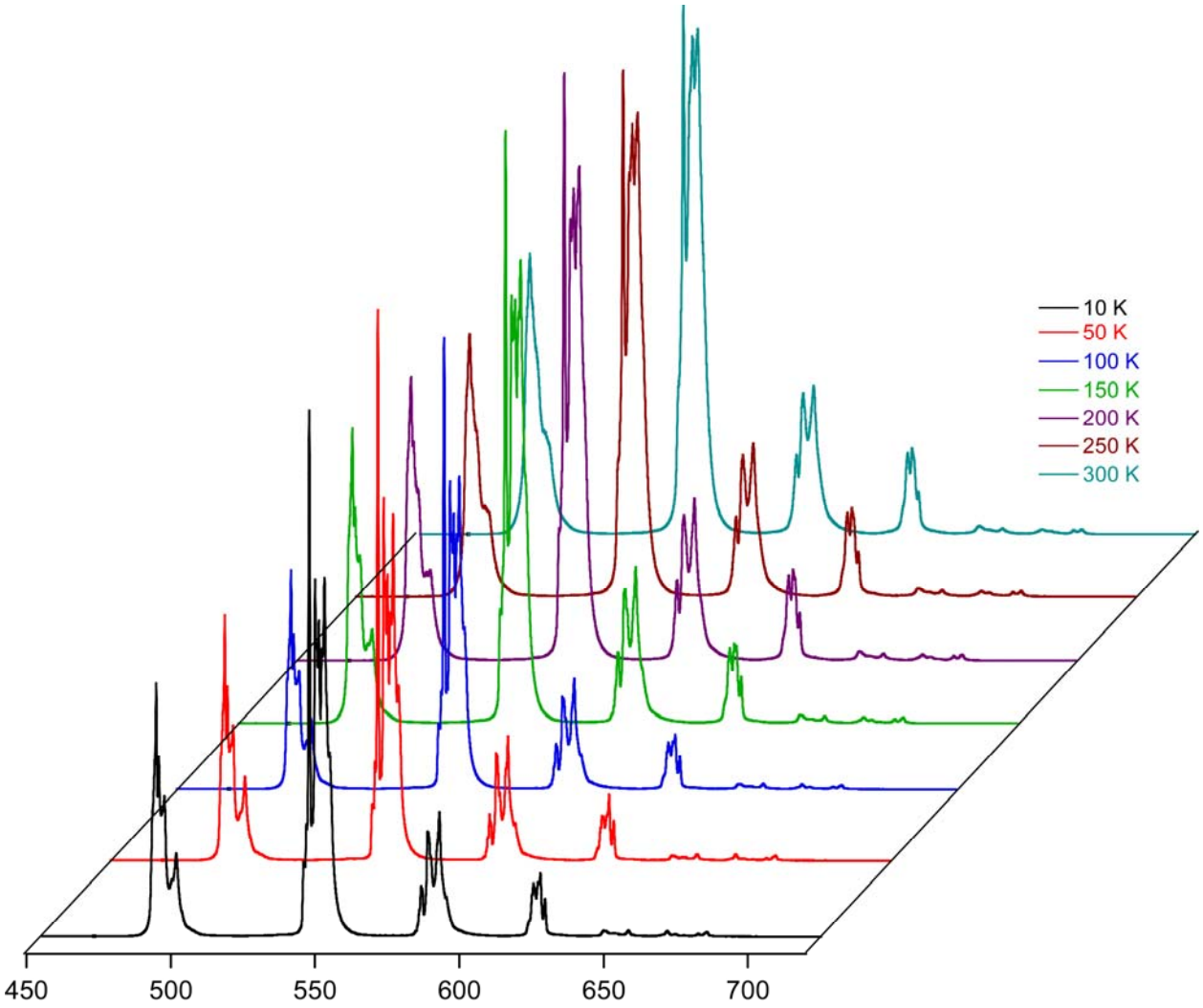

Figure S16. Thermal evolution of the emission spectrum of **2-Tb** excited at 325 nm.

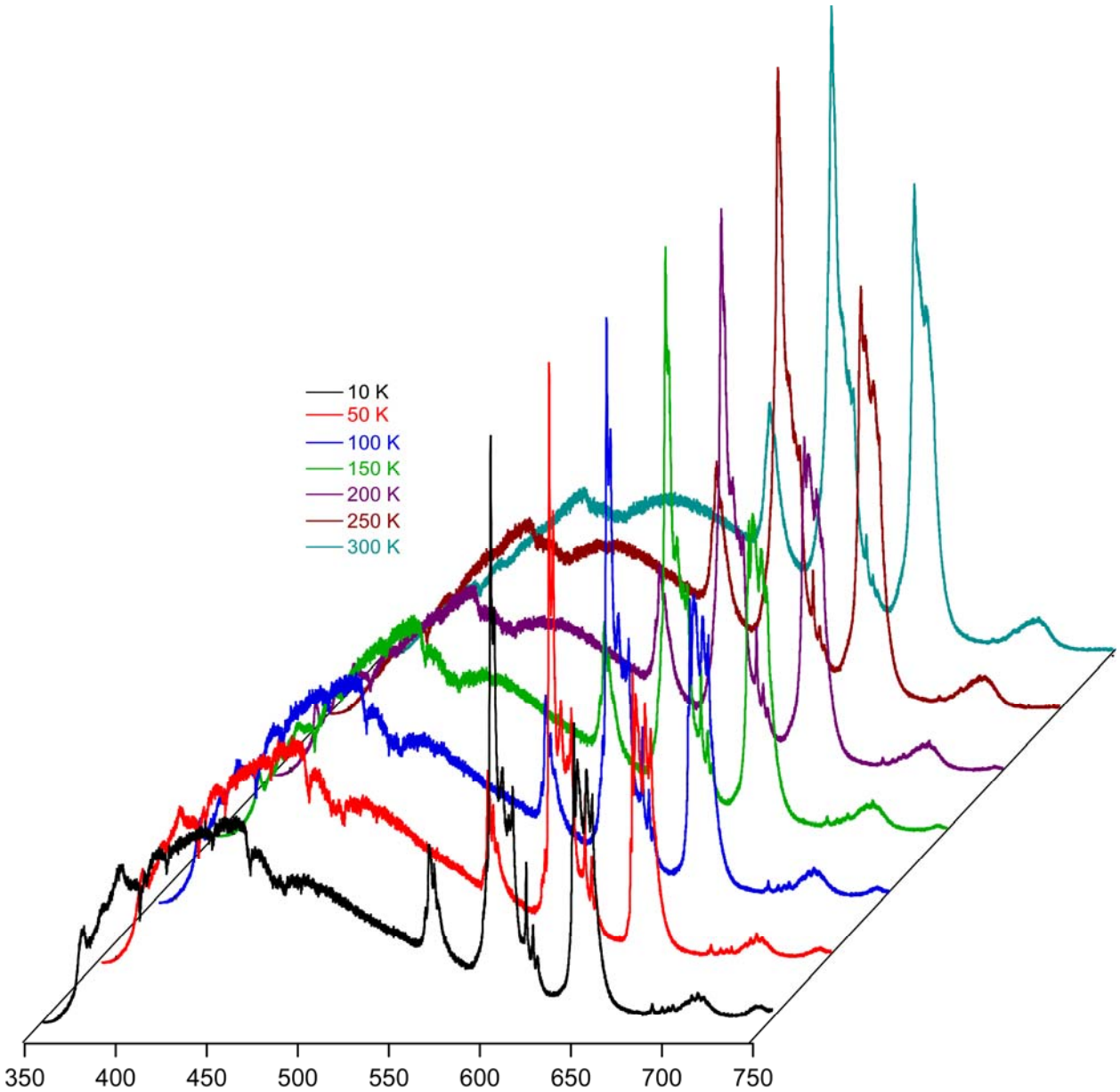

Figure S17. Thermal evolution of the emission spectrum of **1-Sm** excited at 325 nm.

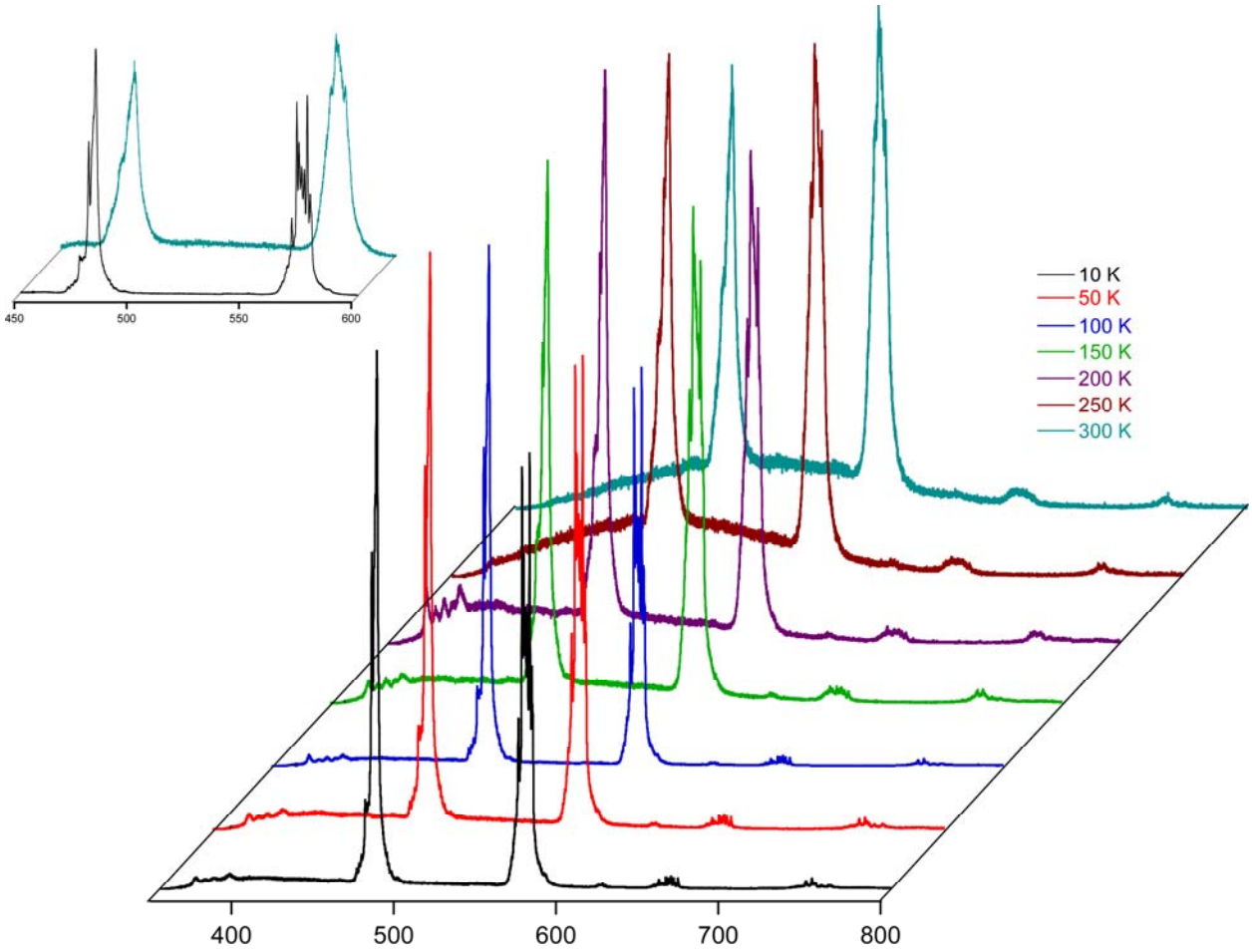

Figure S18. Thermal evolution of the emission spectrum of **2-Dy** excited at 325 nm.

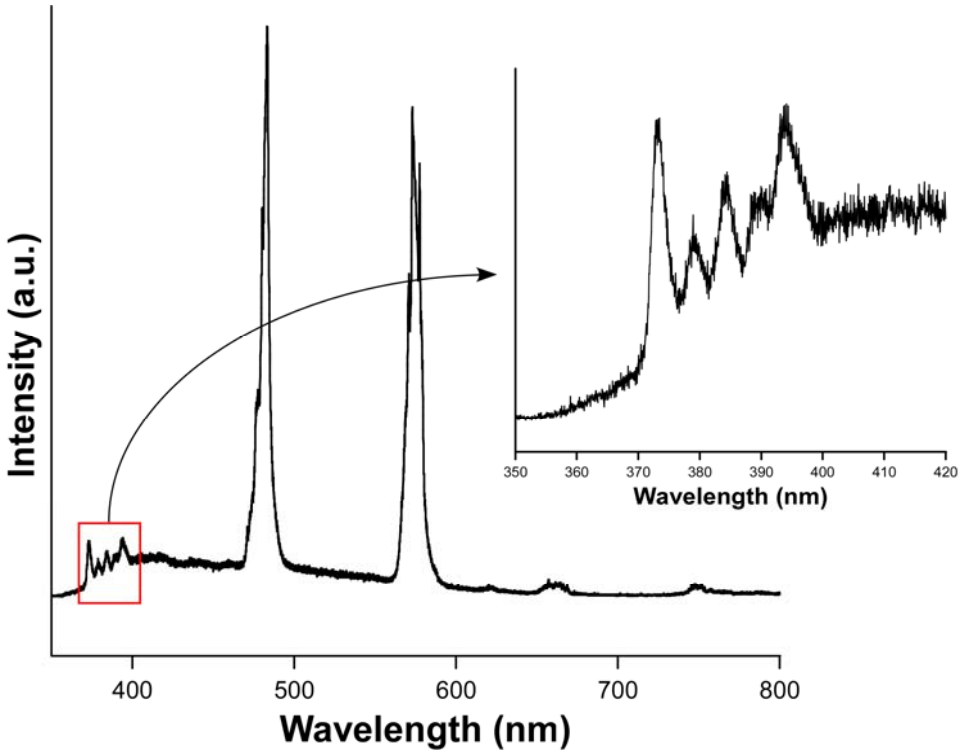

Figure S19. Examination of the ligand fluorescence at 200 K in **2-Dy** compound.

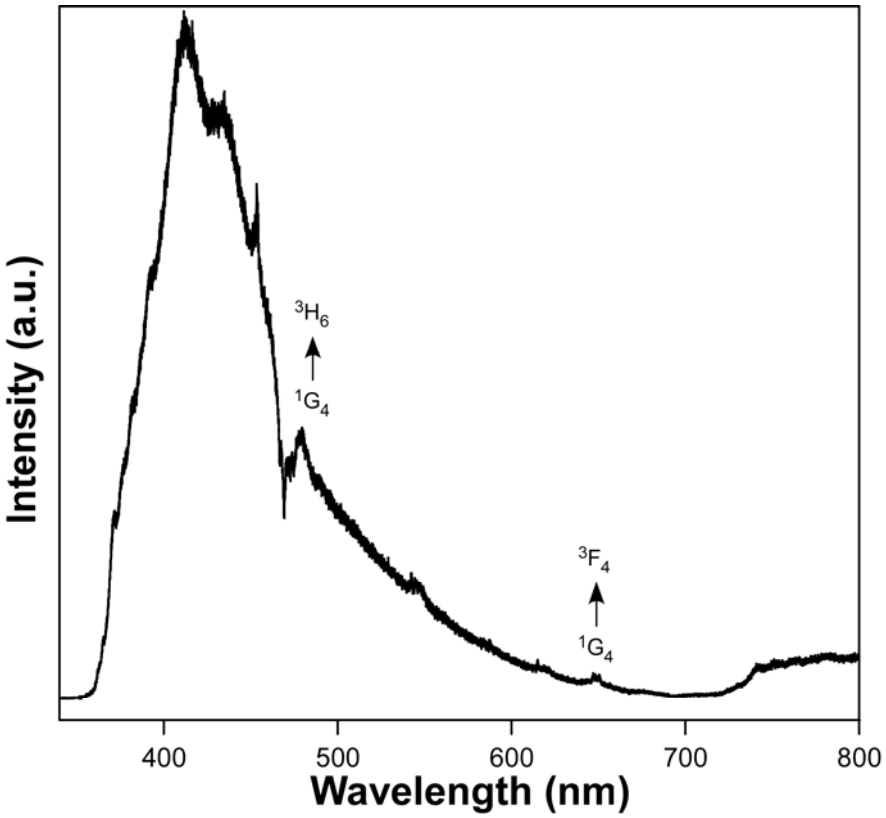

Figure S20. 10K emission spectrum of **2-Tm** excited at 325 nm.

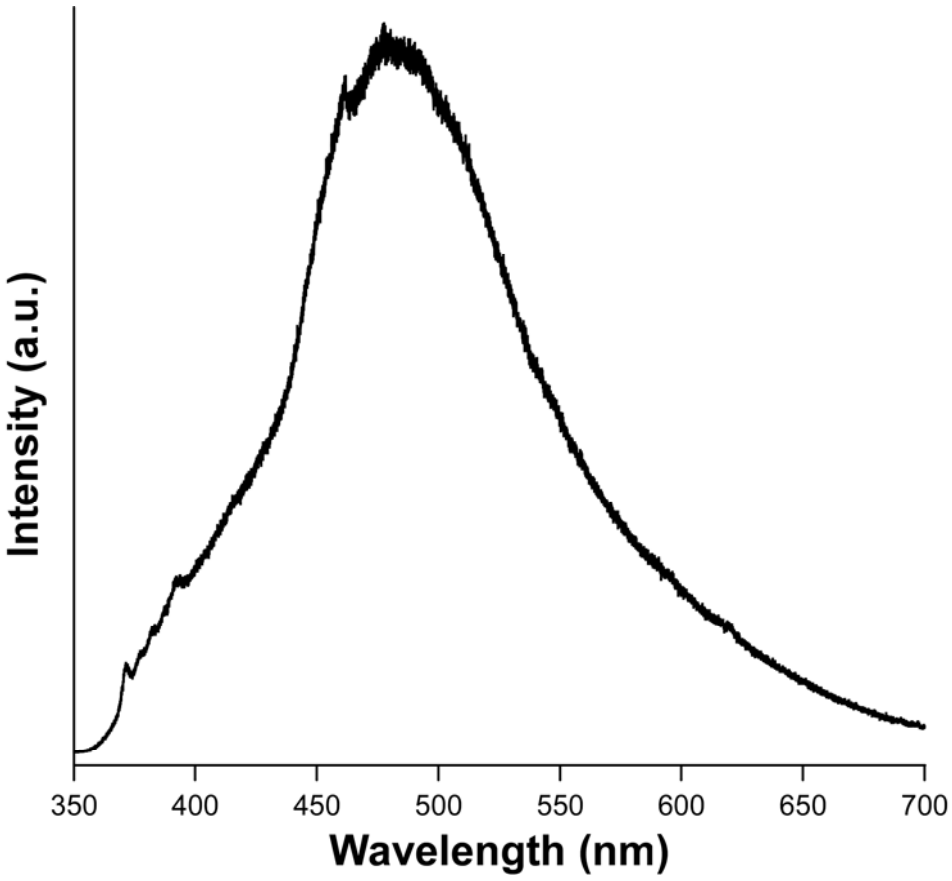

Figure S21. 10K emission spectrum of **2-Gd** excited at 325 nm.

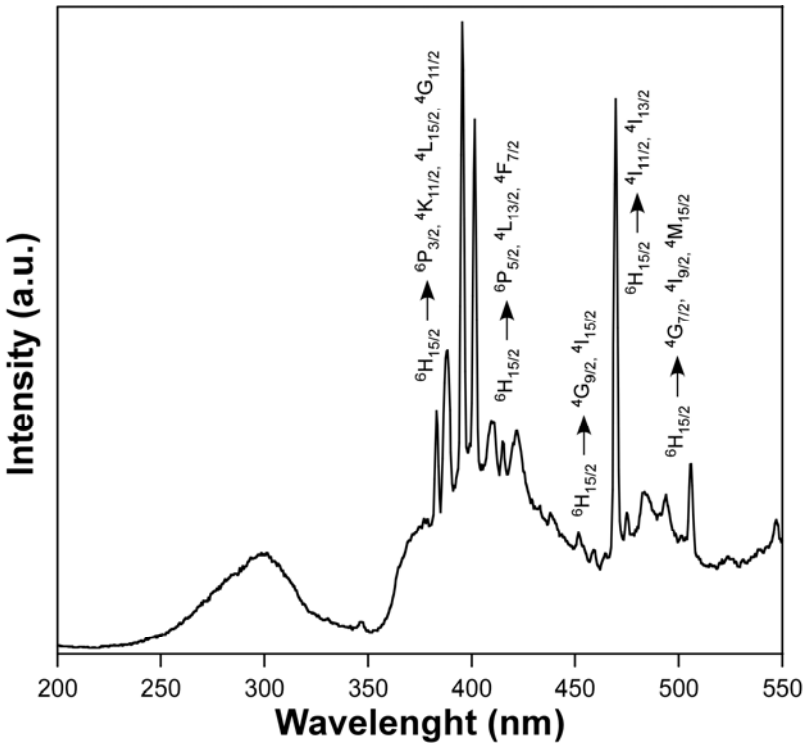

Figure S22. 10K excitation spectrum of **1-Sm** focusing the 595 nm emission line.

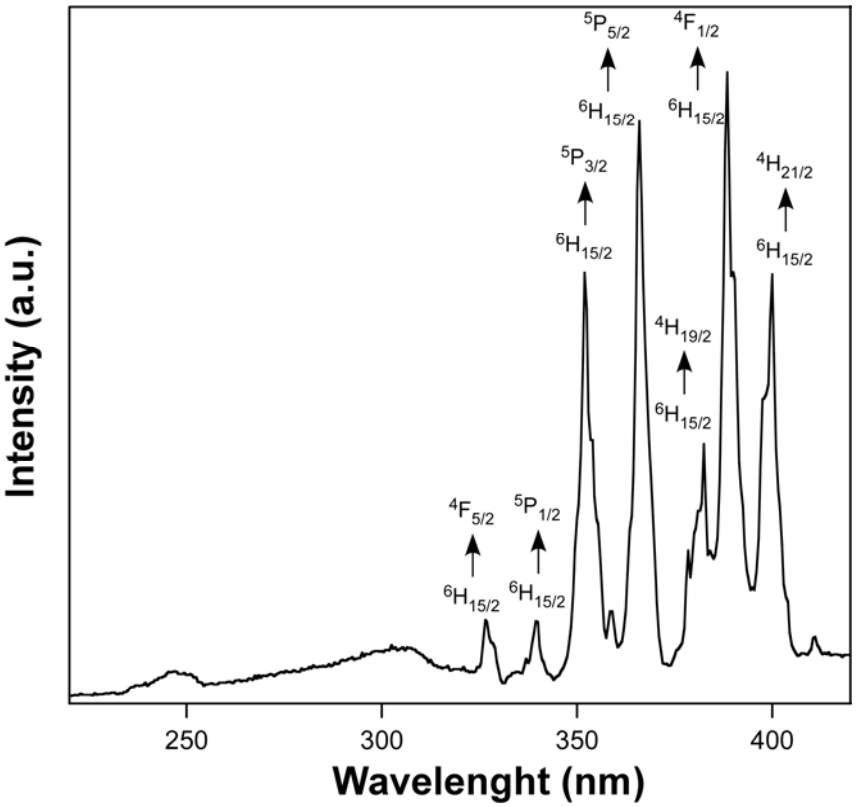

Figure S23. 10K excitation spectrum of **2-Dy** focusing the 483 nm emission line.

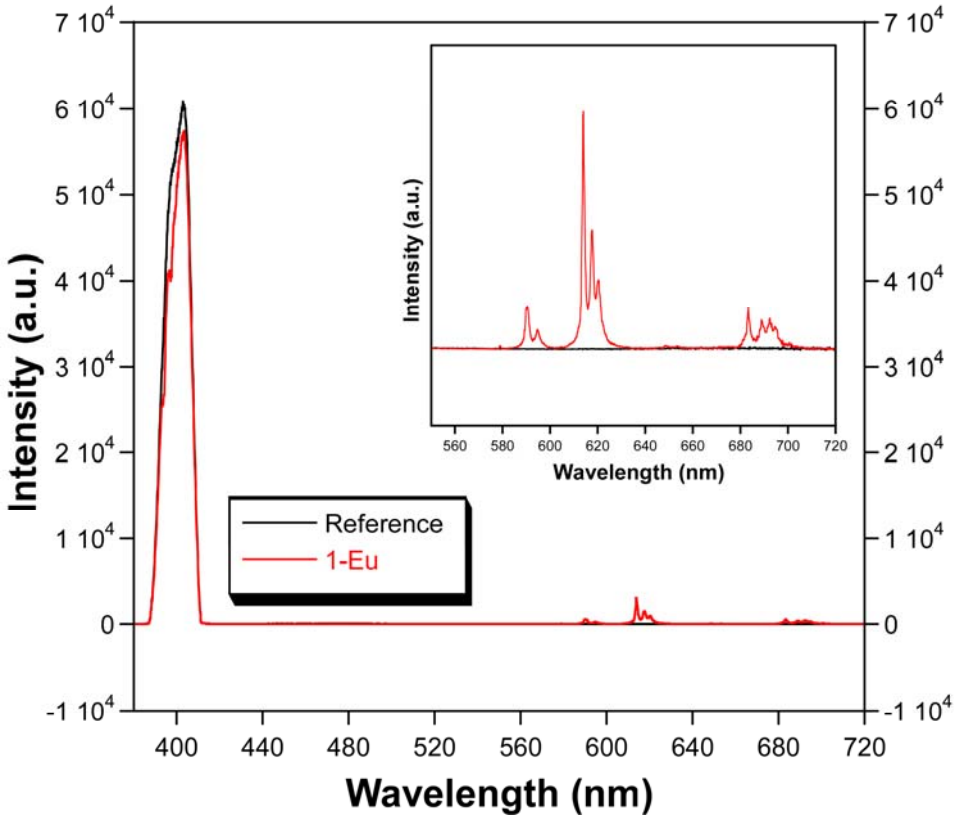

Figure S24. Determination of the quantum yield of compound **1-Eu** at room temperature.

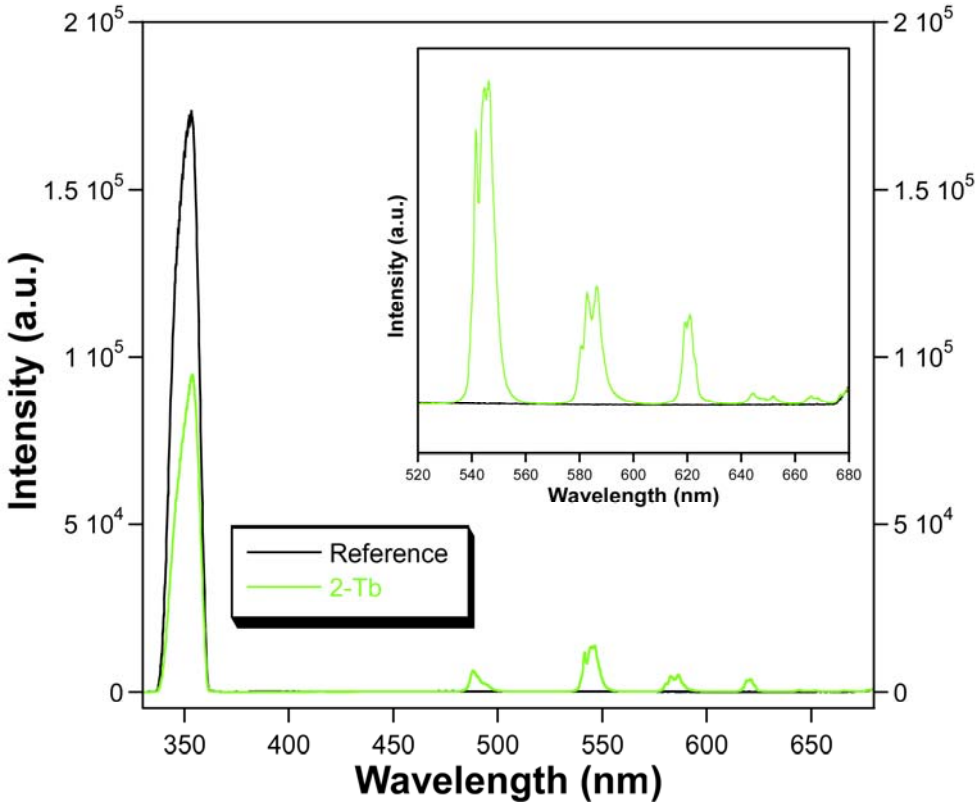

Figure S25. Determination of the quantum yield of compound **2-Tb** at room temperature.

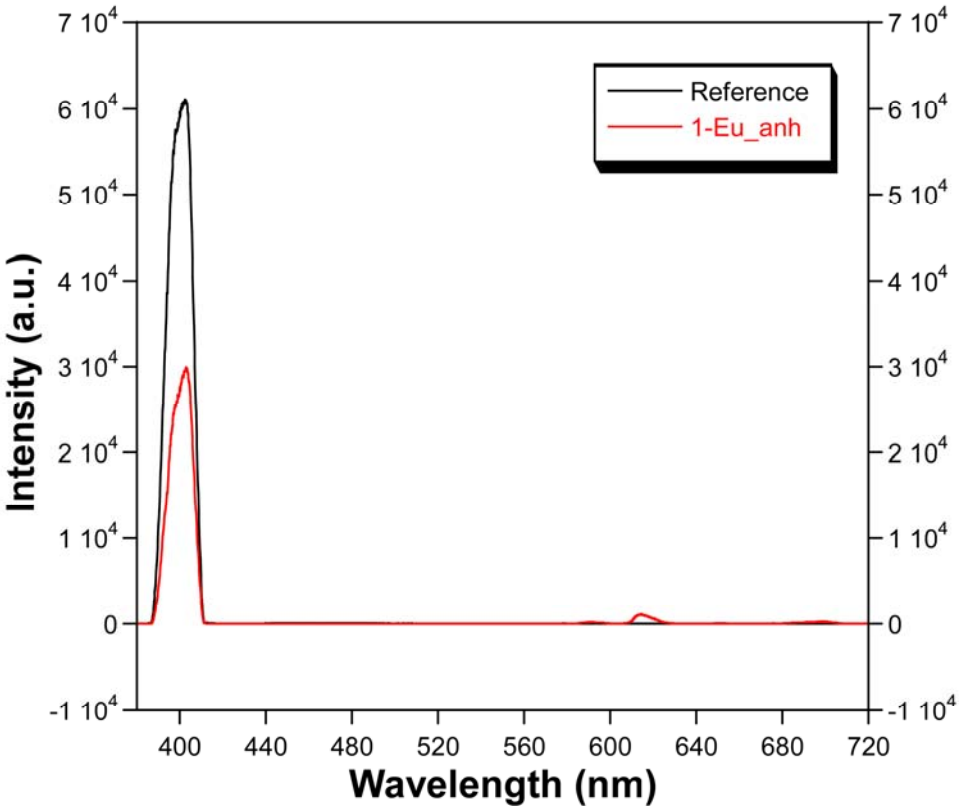

Figure S26. Determination of the quantum yield of compound **1-Eu_anh** at room temperature.

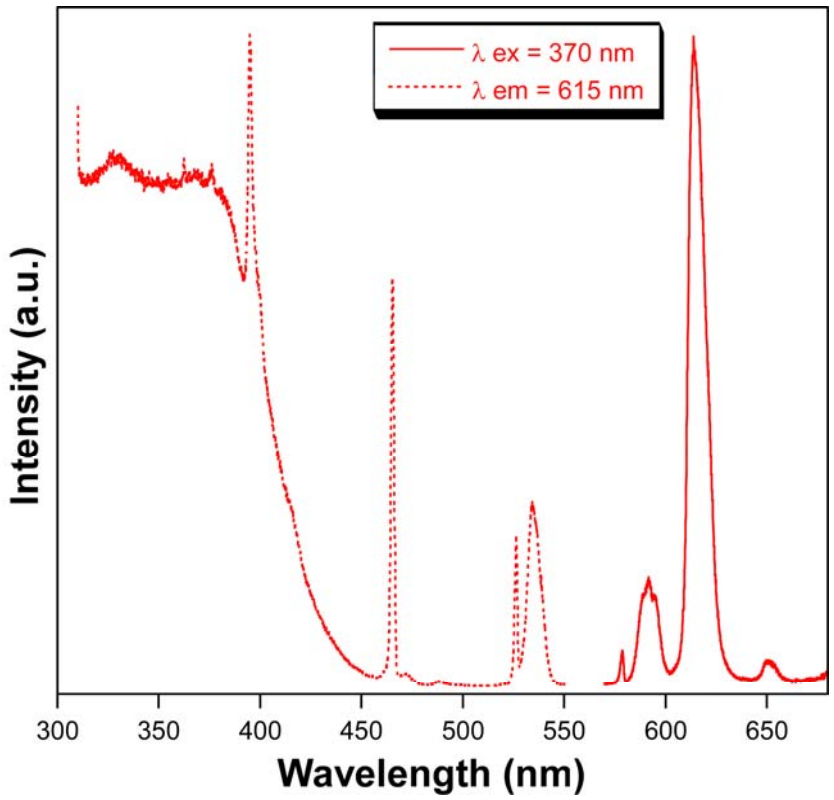

Figure S27. Excitation and emission spectra of **1-Eu_anh** compound at room temperature.

Table S8. Thermal evolution of the visible emission lifetime values of **1-Ln** and **2-Ln** compounds.

	1-Sm		*1-Eu*	*2-Tb*	*2-Dy*
Temp. (K)	***τ₁ (μs) / Rel.***	***τ₂ (μs) / Rel.***	***τ (μs)***	***τ (μs)***	***τ (ns)***
10	1.38(1) / 91.5	12.2(6) / 8.5	538(2)	985(6)	3330(9)
50	1.38(1) / 92.5	13.7(7) / 7.5	535(2)	994(6)	3214(12)
100	1.43(1) / 91.1	12.2(5) / 8.9	493(2)	983(6)	3074(9)
150	1.62(1) 7 91.0	13.1(6) / 8.0	454(2)	984(6)	2983(9)
200	1.75(1) / 91.7	12.6(6) / 8.3	421(2)	1019(5)	2863(9)
250	1.84(1) / 92.8	13.4(6) / 7.2	405(2)	1015(5)	2791(9)
300	1.84(1) / 92.2	12.8(6) / 7.8	400(2)	1022(5)	2700(9)

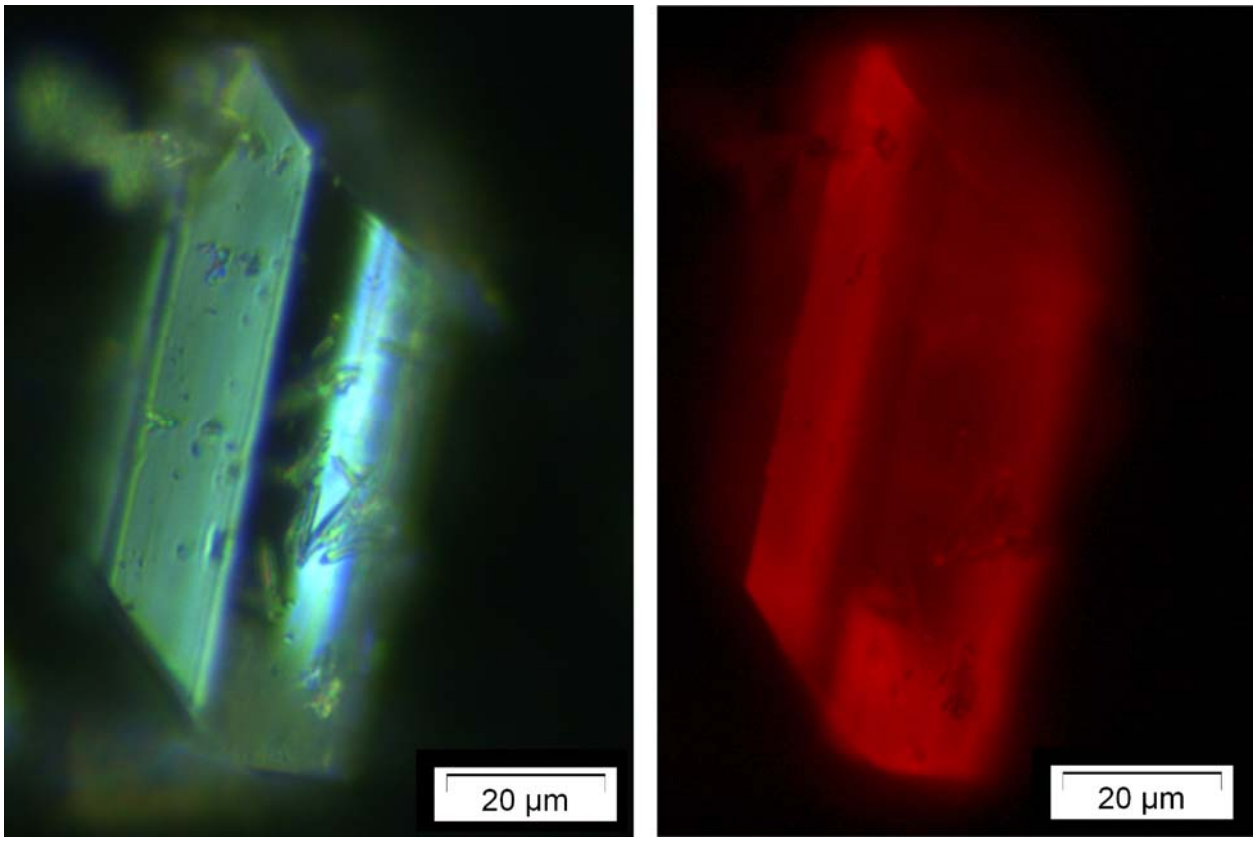

Figure S28. Optical (left) and photo-luminescence (right) images of single crystals of **1-Eu**.

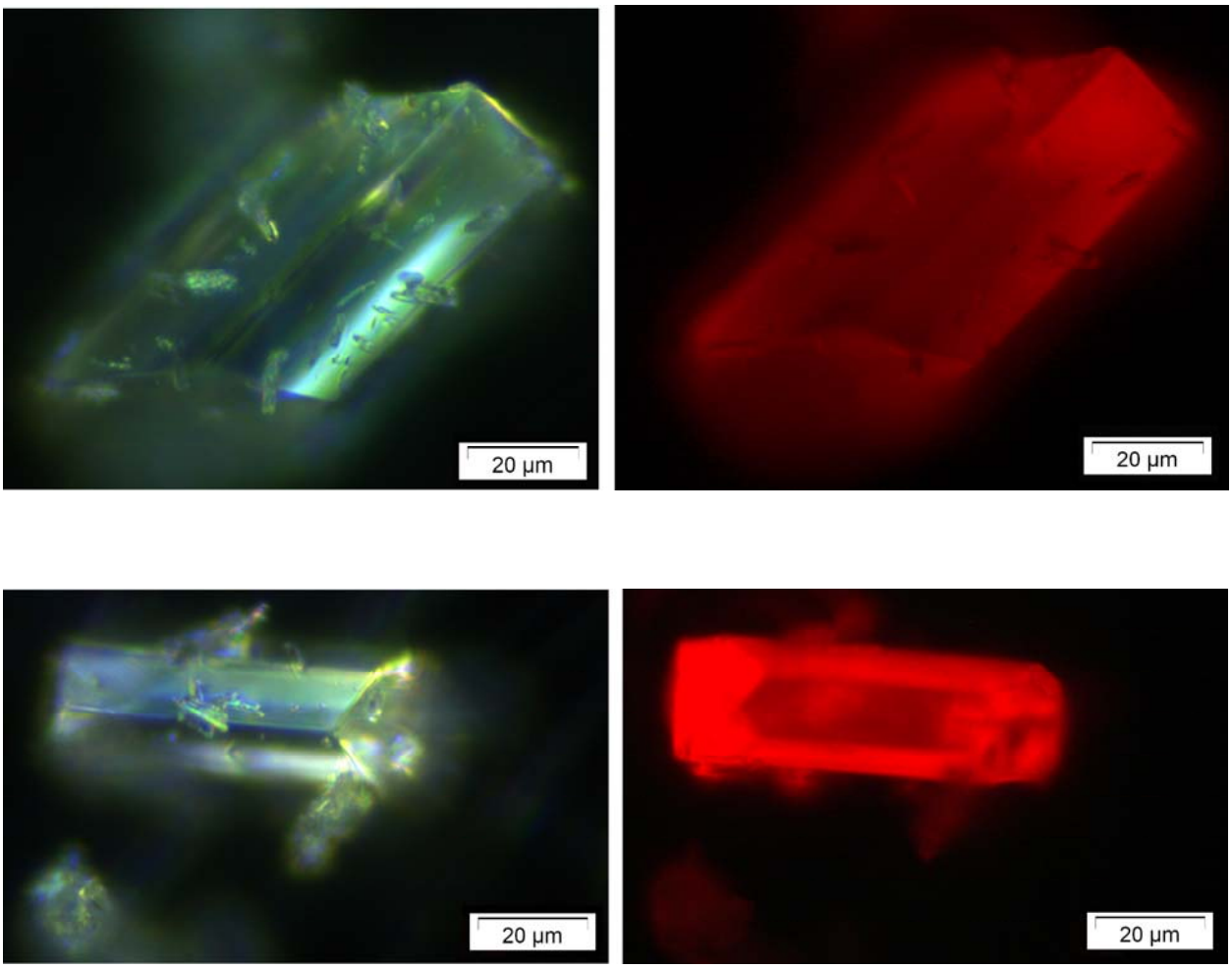

Figure S29. Optical (left) and photo-luminescence (right) images of single crystals of **1-Eu** (cont.).

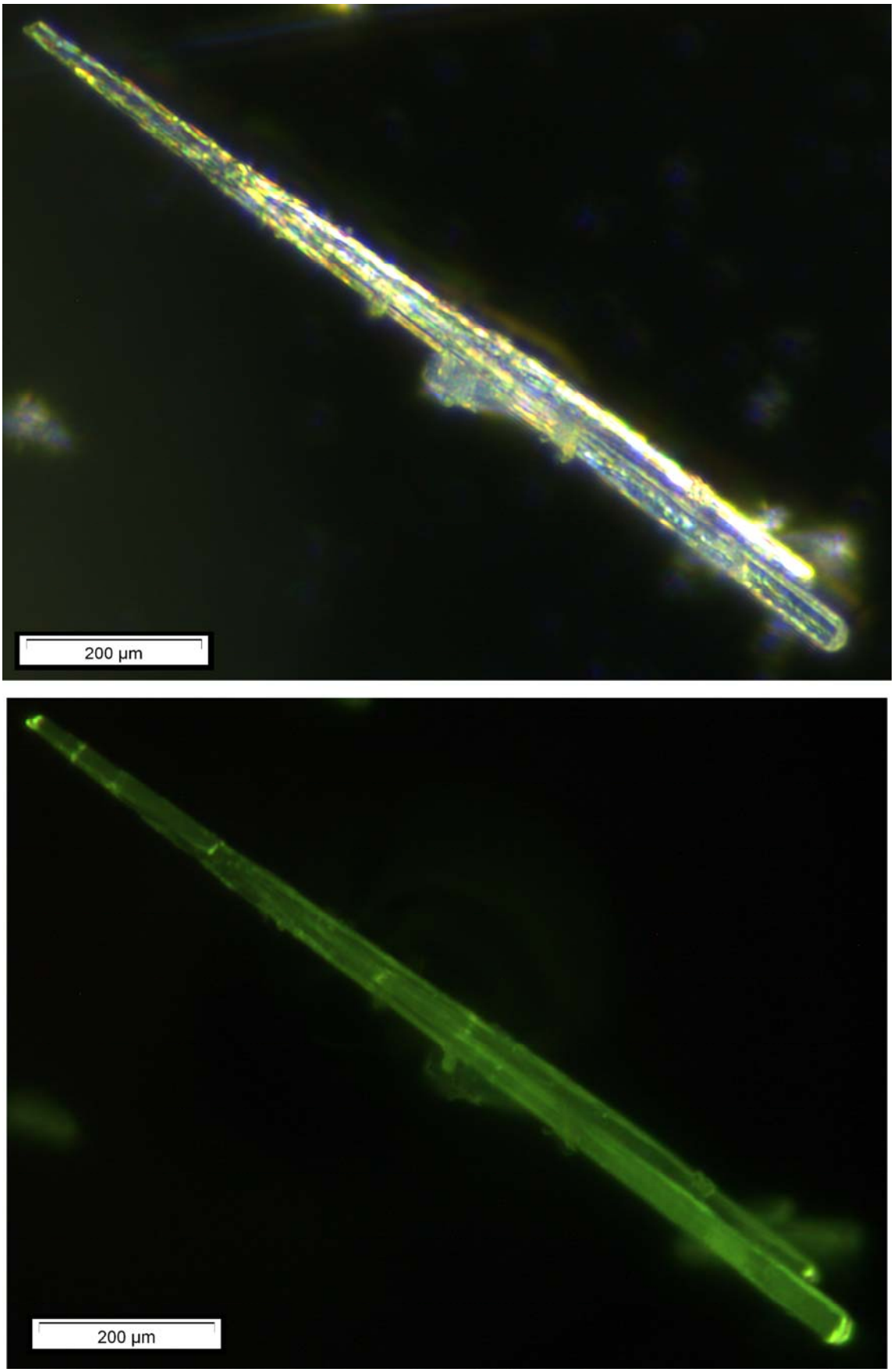

Figure S30. Optical (left) and photo-luminescence (right) images of crystalline agglomerates of **2-Tb**.

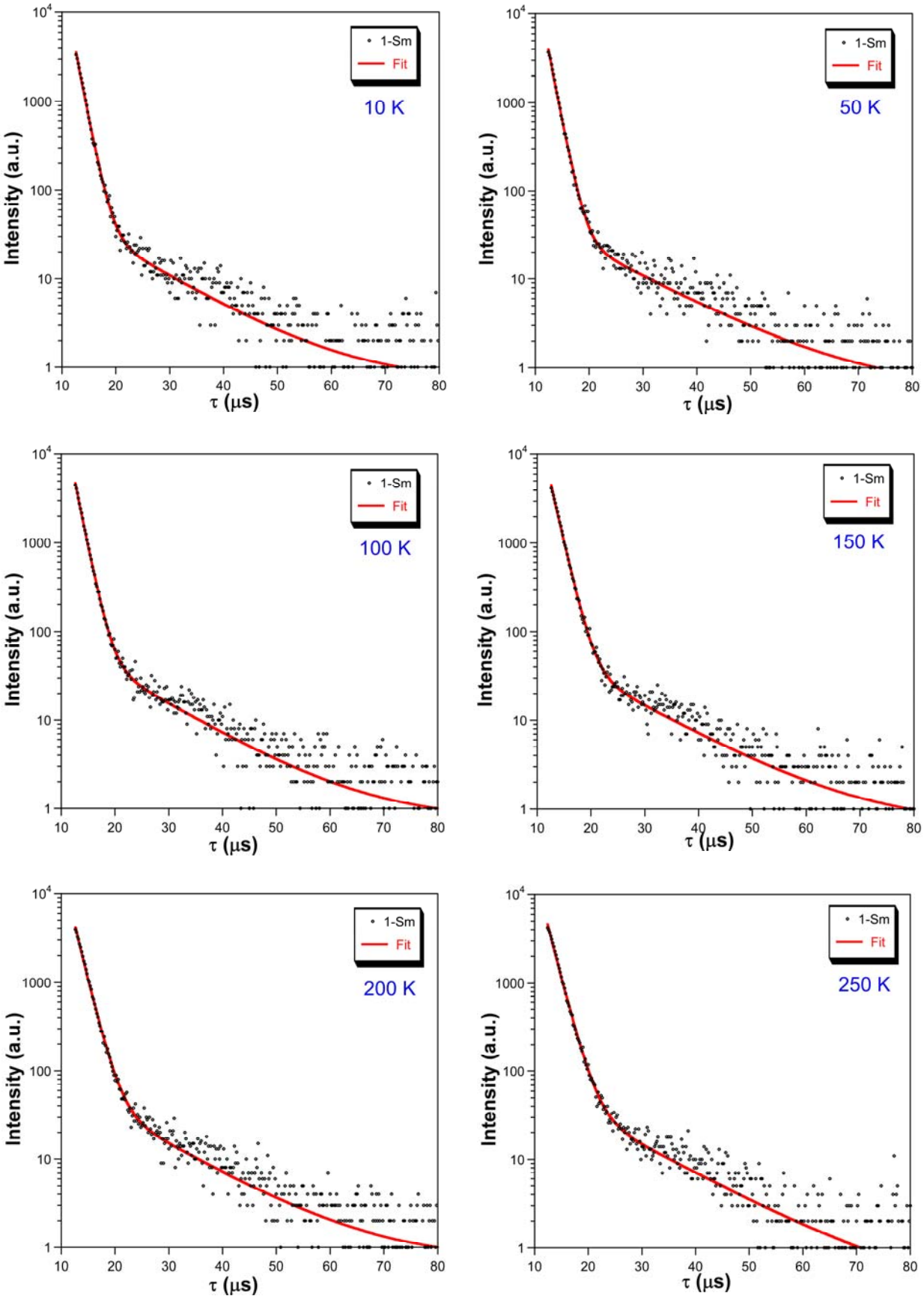

Figure S31. Luminescence decay lifetime fits of **1-Sm** monitored at $^4G_{5/2} \rightarrow {}^6H_{7/2}$ transition.

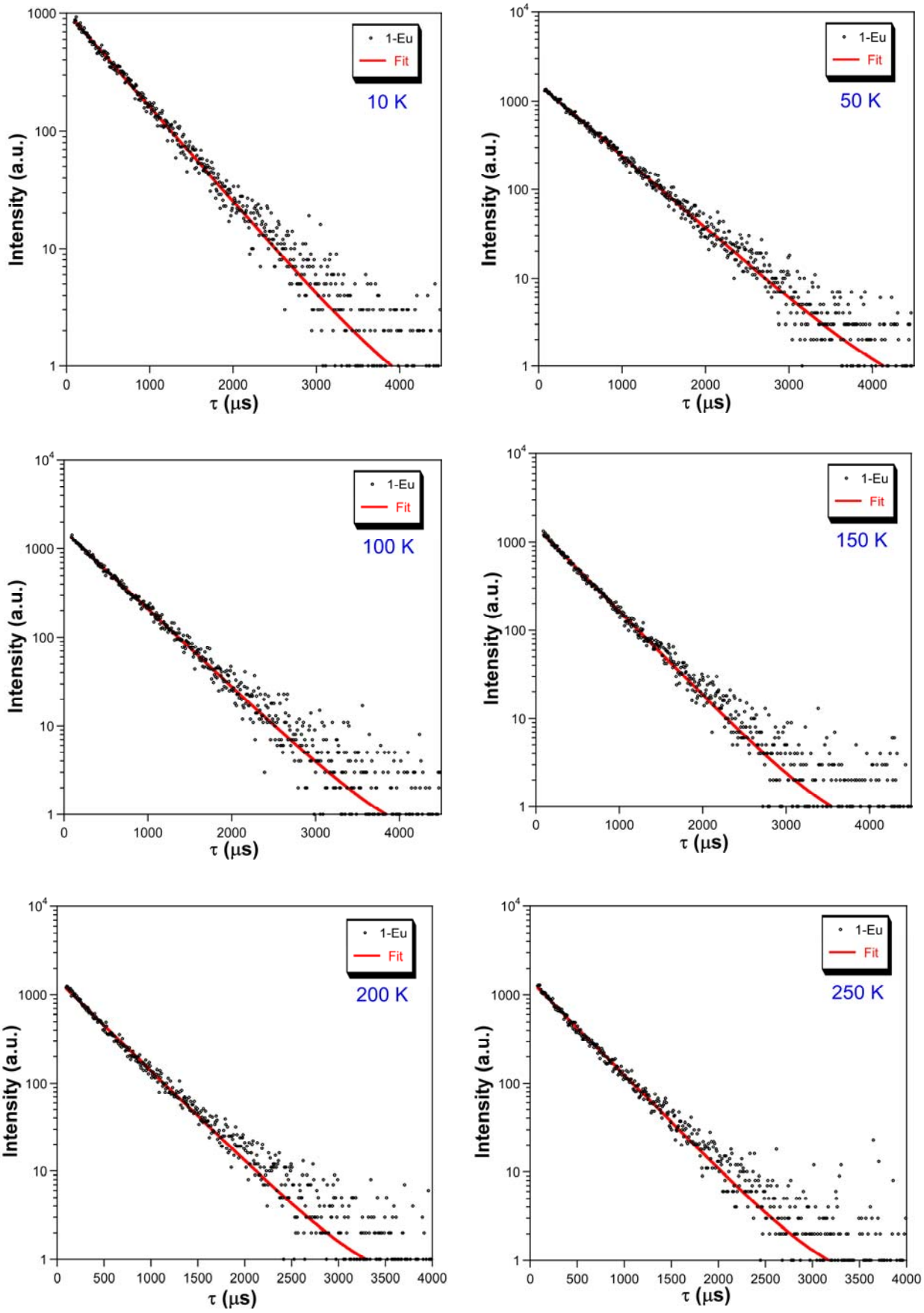

Figure S32. Luminescence decay lifetime fits of **1-Eu** monitored at $^5D_0 \rightarrow {}^7F_2$ transition.

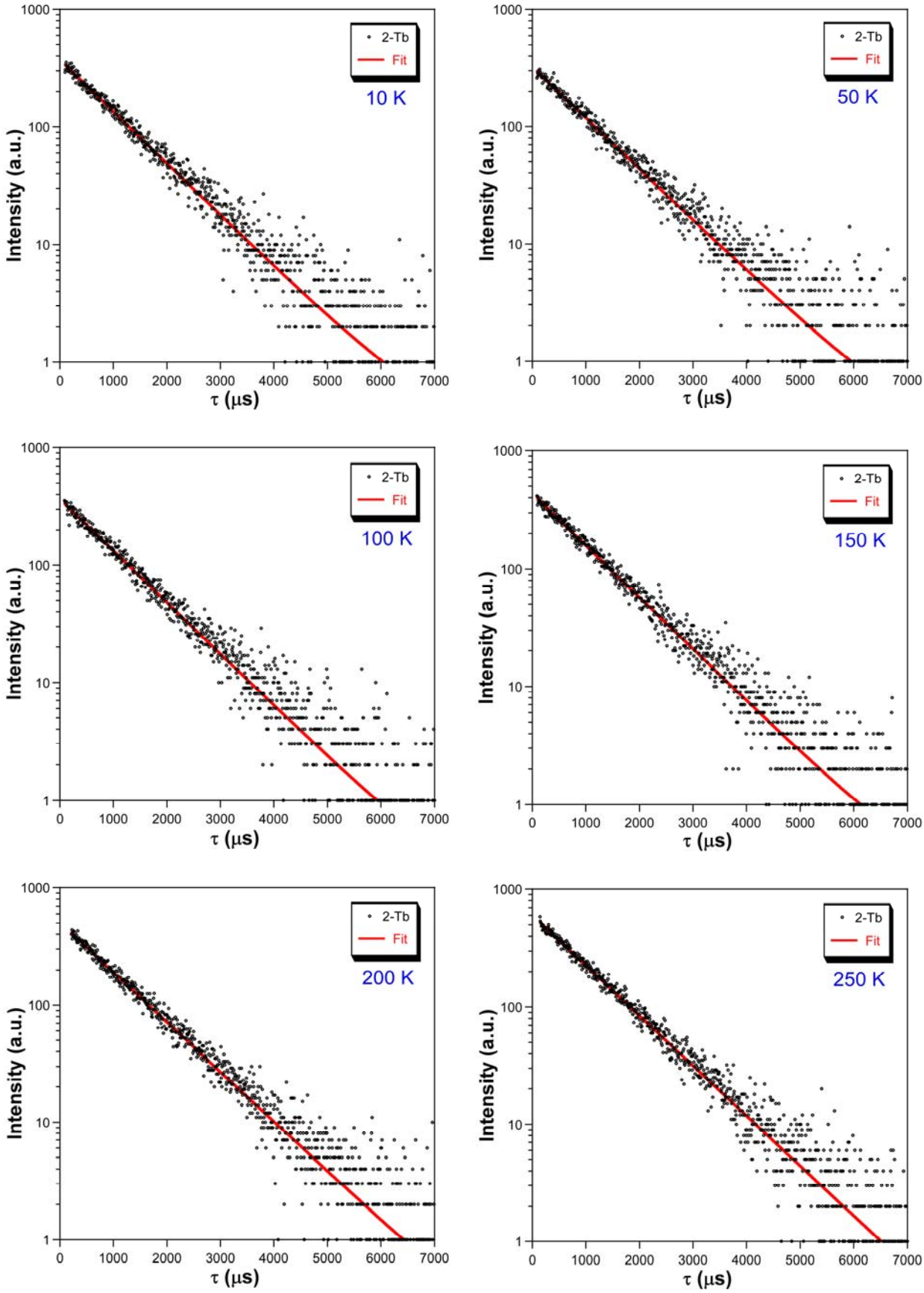

Figure S33. Luminescence decay lifetime fits of **2-Tb** monitored at $^5D_4 \rightarrow {}^7F_5$ transition.

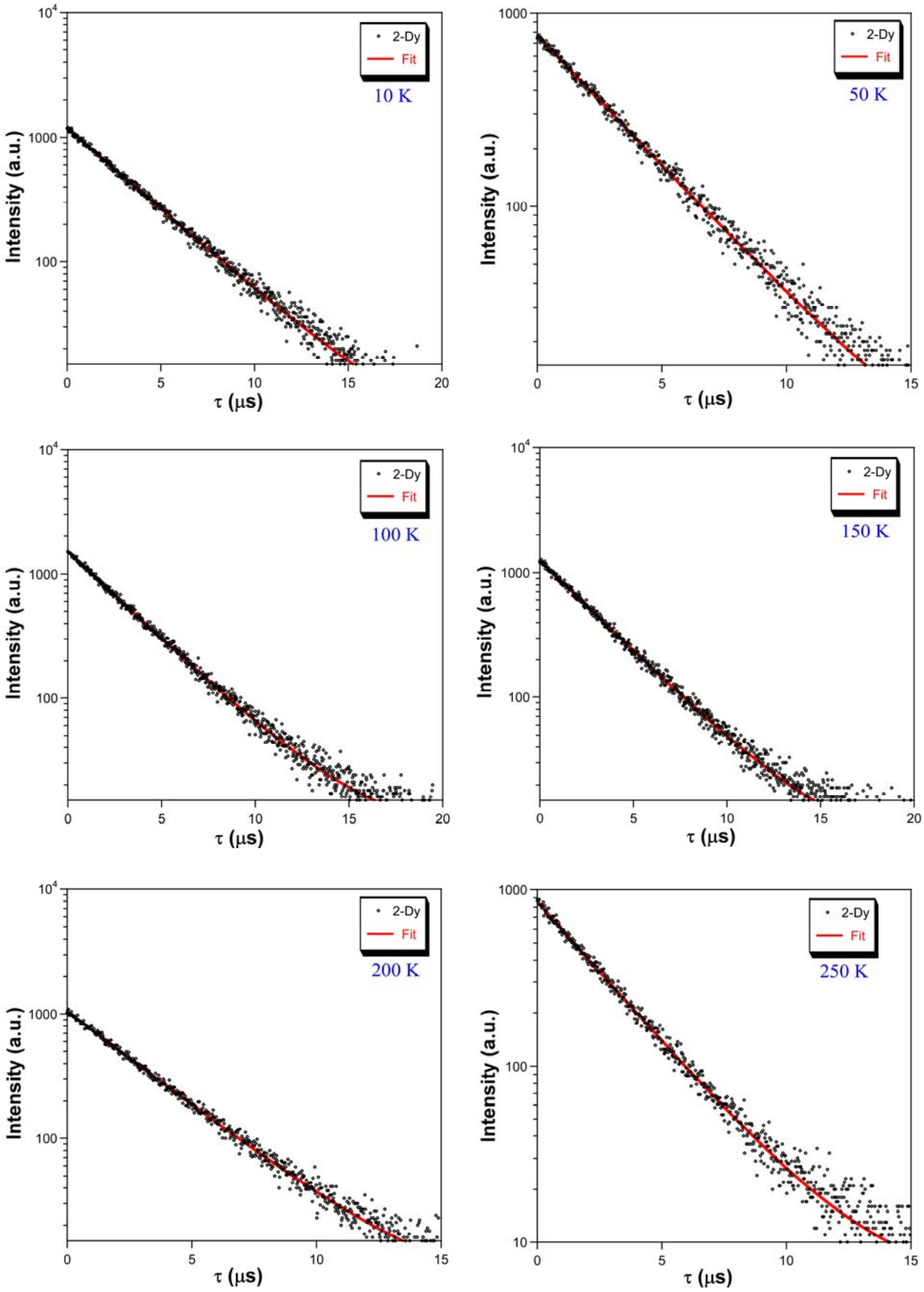

Figure S34. Luminescence decay lifetime fits of **2-Dy** monitored at $^4F_{9/2} \rightarrow {}^6H_{15/2}$ transition.

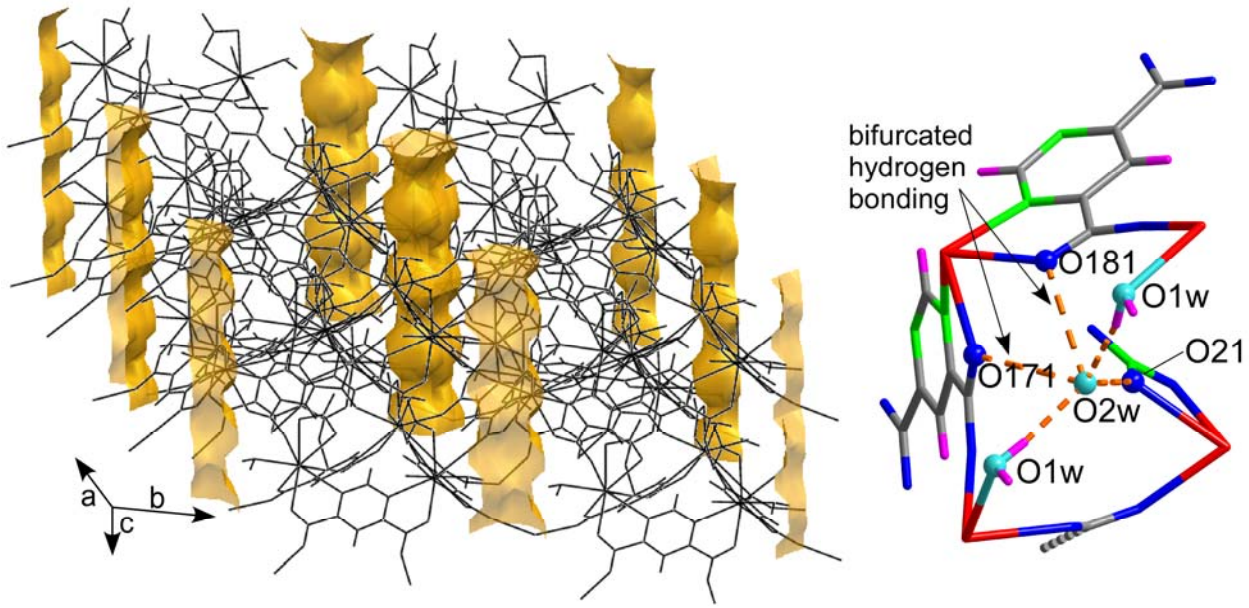

Figure S35. Channels of the **2-Gd** compound with hydrogen bonding interactions.

Table S9. Hydrogen bonding interactions (Å, º) of **1-La** compound.[a]

D–H···A[b]	*D–H*	*H···A*	*D···A*	*D–H···A*
O1w–H11w···O23d	0.85	2.04	2.884(3)	169.5
O1w–H12w···O24e	0.86	2.08	2.922(3)	169.7

[a] Symmetry codes: (d) –x + 1/2, y + 1/2, –z + 3/2; (e) x + 1/2, –y + 3/2, z + 1/2. [b] D: donor. A: acceptor.

Table S10. Hydrogen bonding interactions (Å, º) of **2-Gd** compound.[a]

D–H···A[b]	*D–H*	*H···A*	*D···A*	*D–H···A*
O1w–H11w···O2w	0.86	1.90	2.749(4)	169.6
O1w–H12w···O2wd	0.86	1.90	2.752(4)	171.5
O2w–H21w···O213e	0.90	2.07	2.916(4)	157.1
O2w–H21w···O171f	0.94	2.23	3.034(5)	142.0
O2w–H22w···O181c	0.94	2.23	3.034(5)	142.4

[a] Symmetry codes: (d) –y, x – y, z; (e) y, –x + y, z + 1/2; (f) y, –x + y, z – 1/2. [b] D: donor. A: acceptor.

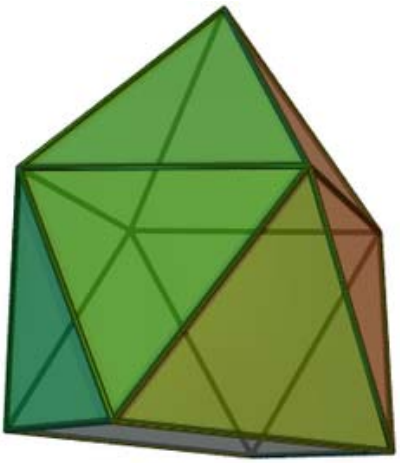

JGSP / Johnson gyroelongated square pyramid

JGSB / Johnson gyroelongated square bipyramid

Figure S36. Ideal shapes with nine vertices (abbreviation / full name).